Fermi National Accelerator Laboratory

FN-433
2020.000

FNAL COLLIDER PHYSICS ON AN ABACUS

D. Green
Fermi National Accelerator Laboratory, Batavia, Illinois 60510

June 1986

Operated by Universities Research Association Inc. under contract with the United States Department of Energy

FNAL COLLIDER PHYSICS ON AN ABACUS

D. Green

Fermilab

Abstract

This note consists of a distillation of a set of academic lectures given to graduate students. The goal is to provide hand calculated estimates good to an order of magnitude for all Fermilab Collider physics processes of interest.

Introduction

The Fermilab TeV-I program consists of experiments in several intersection regions. There are an initial quark search experiment (E-713), an experiment on elastic scattering (E-710), a search for formation of a quark-gluon plasma (E-735) and two high luminosity general purpose detector experiments (E-740, E-741). Because of the breadth of the program, it seemed useful to divide this note into three sections. Section A is a brief review of soft processes, called "ln(s) Physics." The second section consists of an introduction to hard processes, strong interactions and jets. Finally, the third section is an introduction to hard scattering between constituents in electroweak processes.

The references which are included for each of the three sections are meant only to be representative. They reflect the limitations of the author, and not the availability of many excellent review articles. The vast majority of the figures are taken from these references. No claim to completeness or exact calculation is made. The purpose of the note is merely to give an order-of-magnitude familiarity to the physics of the Fermilab $\bar{p}p$ Collider.

A. ln(s) Physics

Total cross section

The parameter which defines how rare a cross section one can study is the luminosity, which relates the cross section to the reaction rate. The design luminosity for TeV I is $10^{30} cm^{-2} sec^{-1}$. For example, an inelastic cross section of 50 millibarns will have an interaction rate of 50 kilocycles. The relationship between rate, luminosity and cross section is given in Eq. A.1.

$$R = L\sigma \qquad \text{A.1}$$

The simplest quantity to measure is the total cross section which measures the total probability for an interaction to occur. As one can see in Figure A.1 the total cross section is rising as the energy varies from the ISR energy regime to the CERN $\bar{p}p$ Collider. This energy rise has a $[\ln(s)]^2$ dependence which is consistent with saturating the Froissart bound. Note that s is implicity normalized as $\ln(s/s_o)$ where s_o is taken to be 1 GeV^2. A parameterization of the total cross section is given in Eq. A.2.

$$\sigma_T = \sigma_0 + a[\ln(s)]^2 \qquad \text{A.2}$$

One can expect that at TeV I the total cross section will be about 75 millibarns.

Elastic scattering

The next simplest process that one can measure is elastic scattering. The only variable is the momentum transfer t. There is a relationship called the optical theorem which relates the total cross section to the imaginary part of the forward elastic amplitude. In other words one is relating the total probability of losing the beam, σ_T, to the forward elastic amplitude. This implies a relationship between

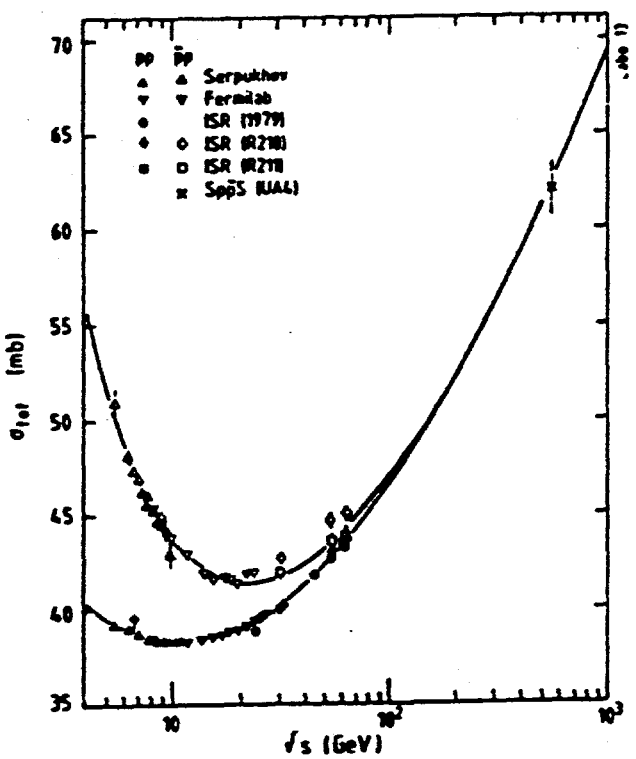

A.1 Total pp cross section as a function of $\sqrt{s}$.

the elastic differential cross section at 0° and the square of the total cross section. The relationship is given in Eq. A.3. In this equation the parameter ρ is the ratio of the real to the imaginary part of the elastic scattering amplitude.

$$d\sigma_{EL}/dt|_{t=0} = (1+\rho^2)\sigma_T^2/16\pi \qquad \text{A.3}$$

For example if ρ is 0 and the total cross section is 40 millibarns then the elastic scattering differential cross section at $t = 0$ is 80 millibarns per GeV^2. That's called the optical point. It is indicated in Figure A.3.

How do you measure the real part of the amplitude? The standard technique is to use the interference between Coulomb scattering and nuclear elastic scattering. As is indicated in Figure A.2 the Coulomb scattering amplitude squared is proportional to the fine structure constant α^2 and, due to the virtual photon propagator, goes as the reciprocal of t^2. The exact formula is given in the expression shown in Eq. A.4.

$$d\sigma/dt = |A_{EM}|^2 = 4\pi\alpha^2/t^2 \qquad \text{A.4}$$

If you equate the differential cross sections given in Eqs. A.3 and A.4 then the Coulomb and nuclear amplitudes are equal at a momentum transfer squared of 0.002 GeV^2. This means that we expect the interference maximum or minimum between these two amplitudes to occur near this value. Figure A.2 is a plot of the ρ parameter as a function of the center-of-mass energy $\sqrt{s}$. You can see that this crosses zero in the ISR energy region. The reason that ρ gives you additional information is that you can write a dispersion relation between the real and the imaginary parts of the elastic amplitude. Measuring the real part at a lower center-of-mass energy tells you, via the optical theorem, about the behavior of the total cross section at

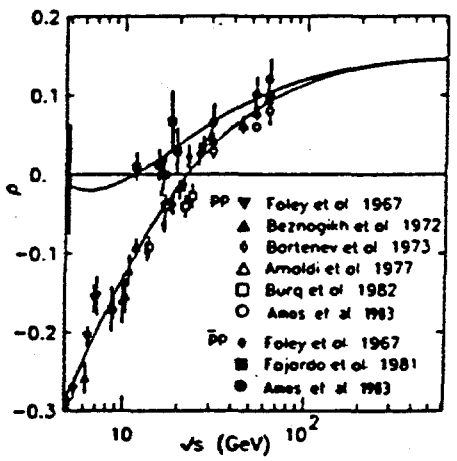

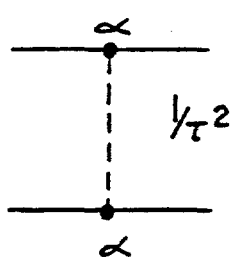

A.2 Real part of the pp elastic amplitude as a function of $\sqrt{s}$.

higher values of s. A simple relationship between ρ and the energy dependence of the total cross section is given below in Eq. A.5.

$$\rho(s) \quad [\pi/2\sigma_T]d\sigma_T/d[\ln(s)]. \qquad \text{A.5}$$

At larger values of momentum transfer we expect that elastic scattering will be dominated by the hadronic interaction. To set the scale for the characteristic hadronic momentum transfer we take a radius for the proton of 1.4 Fermi. Then the characteristic elastic slope which we can see in Fig. A.3 is the radius^2 divided by 4 which is 12 $(\text{GeV})^{-2}$ or, $\langle t\rangle \sim 0.083$ GeV^2, or $\langle q_\perp\rangle \sim 0.29$ GeV. A simple uniform black sphere (radius=R) optical model expression for the elastic differential cross section is given in Eq. A.6.

$$\frac{d\sigma_{EL}}{dt}\Big/\left(\frac{d\sigma_{EL}}{dt}\right)_{\substack{t=0\\ q_\perp^2=t}} \sim \left[\frac{J_1(q_\perp R)}{q_\perp R}\right]^2 \rightarrow \left[e^{-(Rq_\perp/2)^2}\right]_{q_\perp R<<1} \qquad \text{A.6}$$

If you look at Fig. A.3 you can see the optical point and the characteristic exponential fall-off of the elastic scattering cross section with t.

At higher values of t we find diffraction minima; that is we see dips in the cross section at the roots of the Bessel function. At ISR energies this happens at a t of about 1.4 GeV^2 whereas at the CERN collider this happens at about 0.9 GeV^2. In a simple minded way this means that the radius of the proton is changing and is getting larger. This correlates with the fact that the cross section is rising since the cross section is roughly related to the geometric cross section which is $2\pi R^2$. The slope change also indicates that the radius is increasing with $\sqrt{s}$.

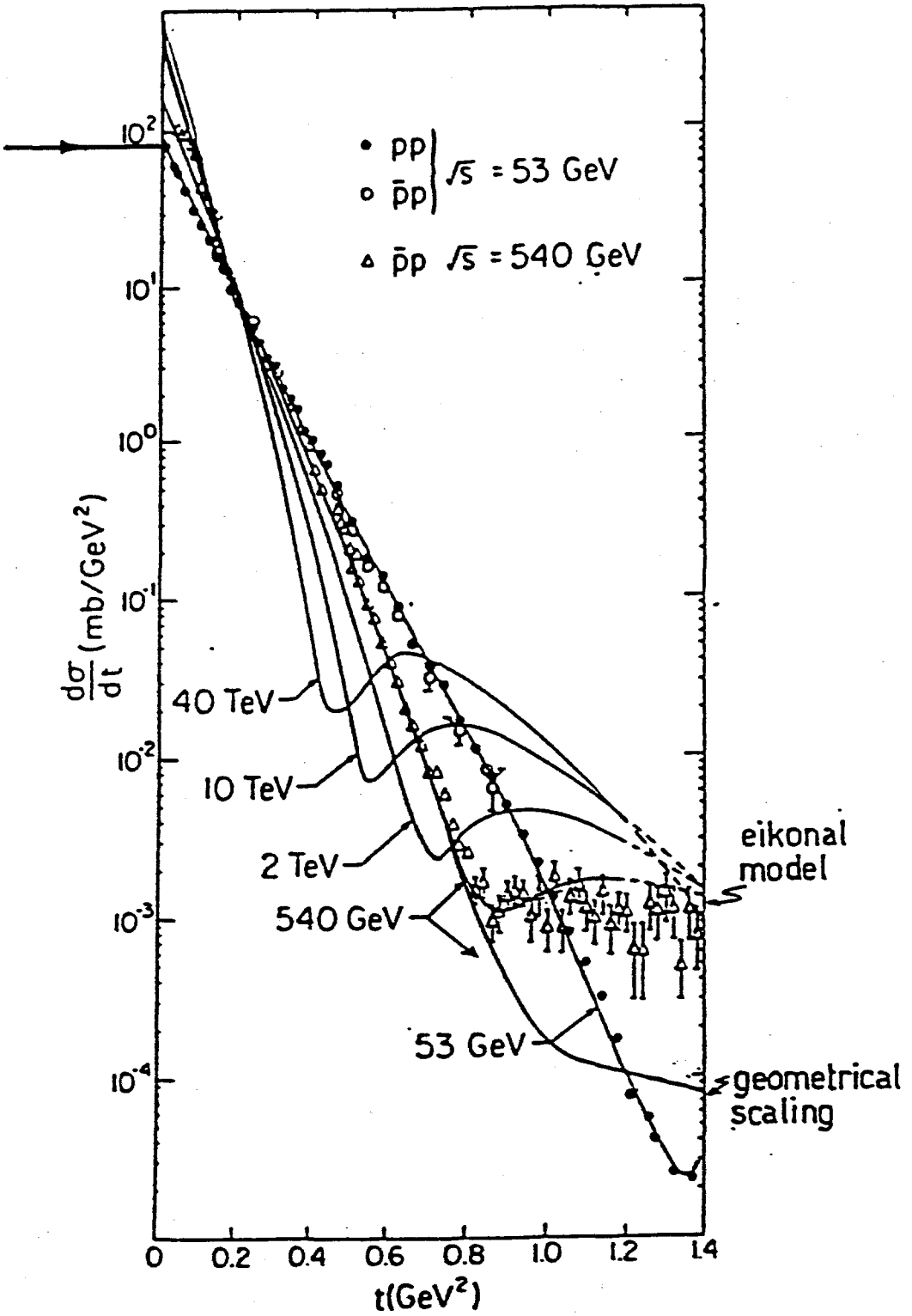

A.3 Elastic scattering differential cross section for $0 < t < 1.4\ (\mathrm{GeV/c})^2$.

In Fig. A.4 we see a layout of the small angle elastic experiment E-710. The goals of this experiment are to measure the real part of the elastic scattering amplitude by measuring the Coulomb interference and to extrapole $d\sigma/dt$ to t=0 to measure the total cross section (see Eq. A.3). We expect the interference maximum to occur at $t=0.002\ GeV^2$. Now, t is approximately $(P_o\theta)^2$. This means a momentum transfer of $q_\perp$=45 MeV which for a beam momentum, P_o, of 1 TeV means an angle of 45 micro radians. Since one can probably get only within a radius of a centimeter and still clear the beam, this means that the detectors are deep in the machine magnet lattice. They would have to be located at a longitudinal distance of ± 220 meters in order to measure in the Coulomb interference region. In fact if you look at Fig. A.4, that is the order of magnitude of the dimensions of the experiment.

Diffractive scattering

After elastic scattering, the next simplest process which has a large cross section is single diffraction. This is a process where one of the projectiles remains intact and the other one fragments into a system of mass M. If you do the kinematics, then momentum and energy conservation yields approximately Eq. A.7. The x value (which is the fraction of the beam momentum in the center of mass carried off by the intact projectile) is related to the mass of the diffracted system and the total center-of-mass energy. Transverse momenta, $q_\perp$, are assumed to be small.

$$2P_o \quad P_o x + \sqrt{(P_o x)^2 + M^2}$$

$$x = 1 - M^2/s \qquad \text{A.7}$$

$$\sqrt{s} = 2P_o$$

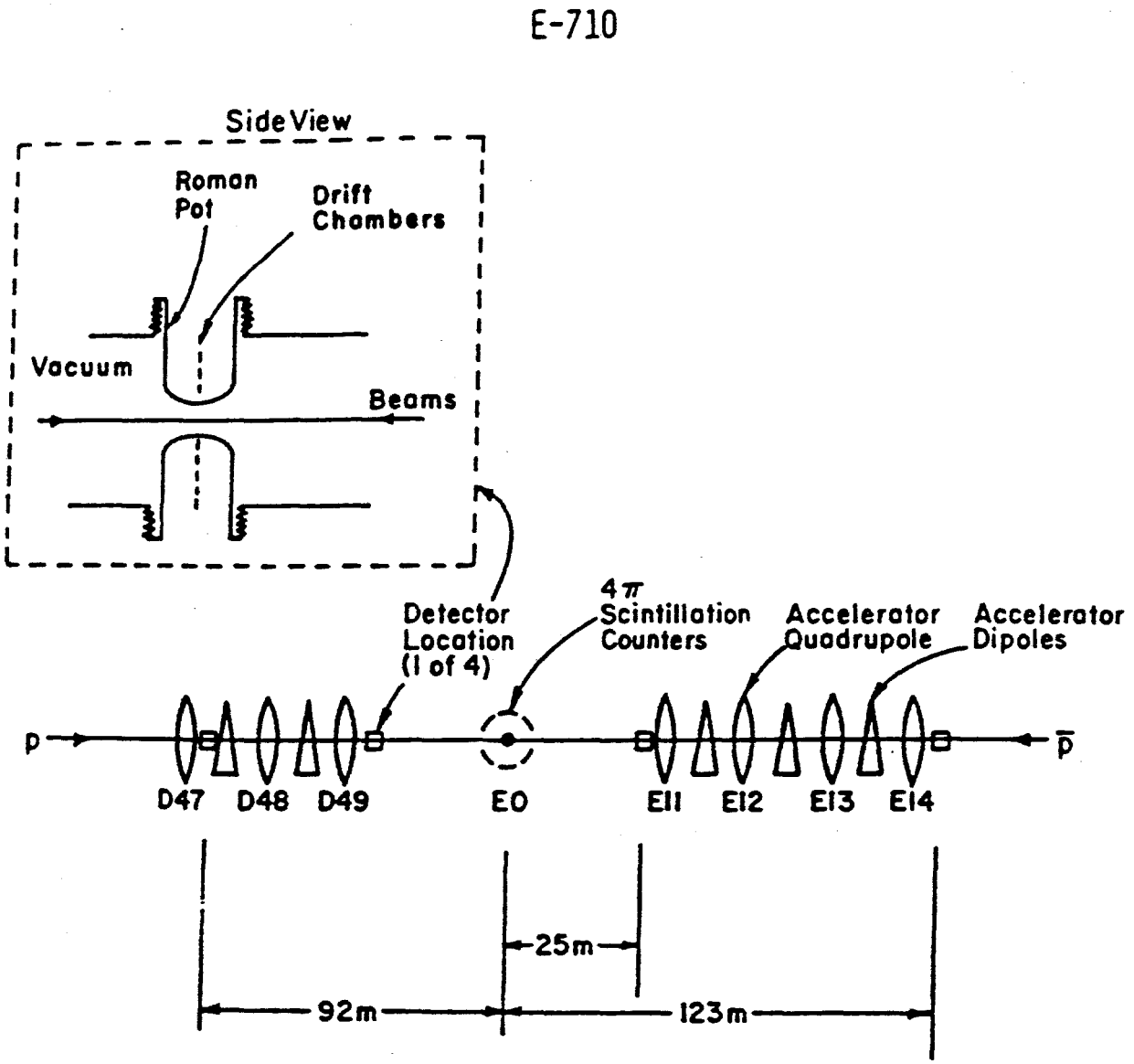

A.4 Layout of E-710 (EØ).

Typical spectra for inelastic protons at ISR energies are shown in Fig. A.5. The vertical scale indicates that this is a copious process because it is millibarns per GeV^2. We can also see that diffraction has the characteristic property of being extremely peripheral. As in elastic scattering, the cross section falls off very rapidly with momentum transfer which indicates scattering from extended objects. Most striking is a sharp diffractive peak at high x; that is proton momenta which are within 1/20 of the original beam momentum. If we define $x > 0.95$ to be diffractive, then at Tevatron collider energies we can diffractively produce masses up to 440 GeV. By using the diffraction mechanism, we can make high masses with large cross sections.

Another purely phenomenological fact about diffraction is that the cross section for diffraction as a function of the square of the diffractive mass goes as $1/M^2$. The scaling property for diffraction is then $M^2 d\sigma/dM^2$ = constant. Integrating the cross section from a minimum value of the mass M_o at the center-of-mass energy s and normalizing it to the total diffractive cross section, σ_D, we get the approximate expression

$$d\sigma_D/dM^2 \sim \frac{\sigma_D}{M^2}\left[1/\ln\left(\frac{x_o s}{M_o^2}\right)\right] \qquad \text{A.8}$$

For example if we take one millibarn for the diffractive cross section, a lower mass M_o of 1.4 GeV and a diffractive system mass of 100 GeV (that means pair production of 50-GeV top quarks) then the diffractive cross section above 100 GeV mass is very substantial. It's 120 microbarns! Now assume that diffraction is flavor blind, which means the Pomeron does not care what the flavor of the quarks is that it produces. In that case, you would expect that the diffractive cross section for $t\bar{t}$ pair production would be about 20 microbarns. This implies an enormous rate at the collider. Where would you look for the reaction products? The three body

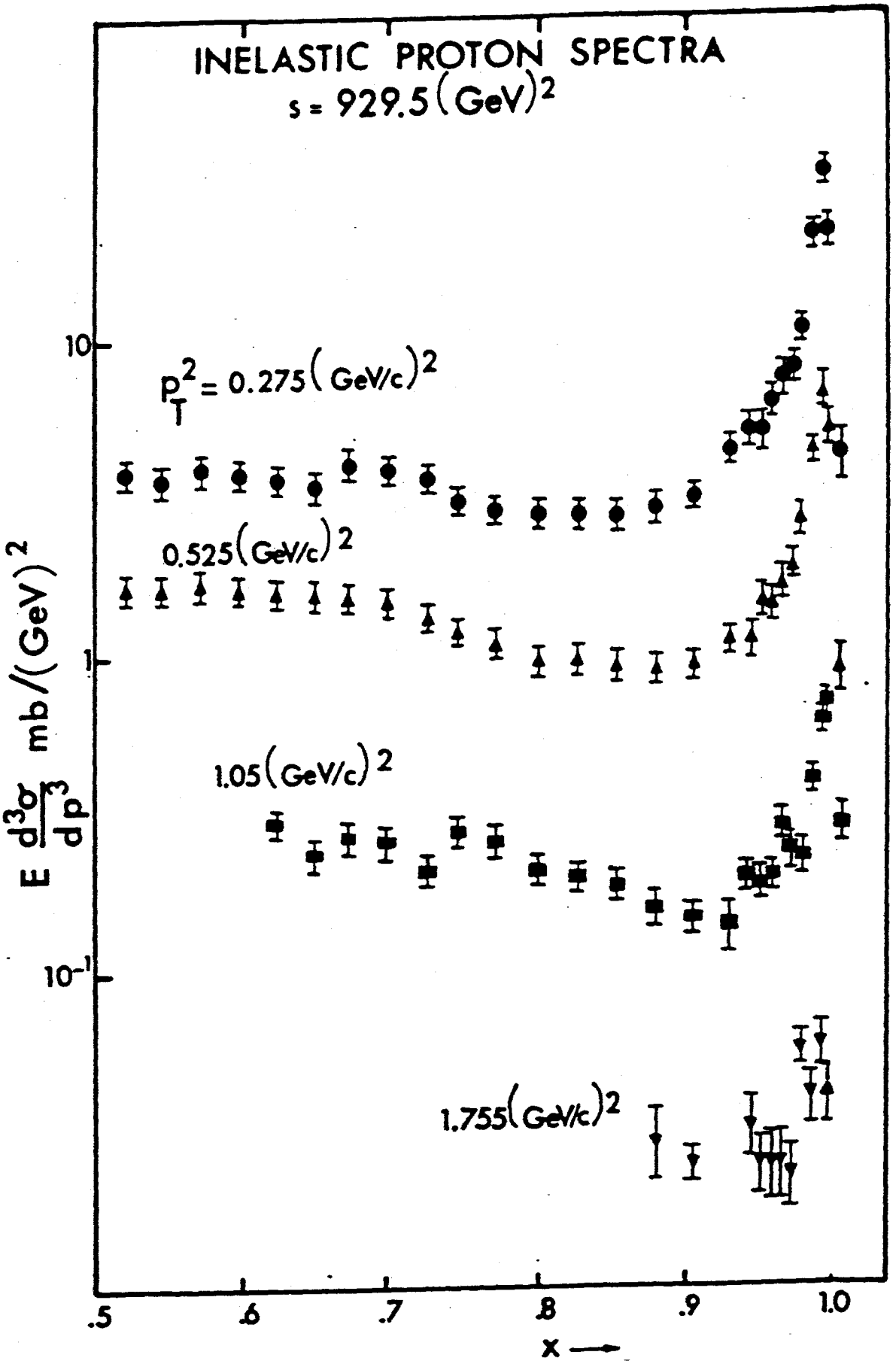

A.5 Inelastic proton spectrum, E $d\sigma/d\vec{P}$ vs x.

semileptonic decay $t \to b\mu\nu$ has a large branching ratio. The muon would have 1/6 of the beam momentum. For 2,000 GeV in the center of mass, with a 50-GeV top mass the muon would have 167-GeV momenta. It would have about 17 GeV of transverse momentum and would come out at about 100 milliradians. That means if you are looking for semileptonic decays of diffractively produced heavy quark pairs you would put up a forward detection system for fairly high-energy muons.

Lorentz invariant cross section

The elastic cross section is reasonably copious, being about 1/4 of the total cross section. The single diffractive and double diffractive cross sections are related by factorization and contribute roughly another 1/8 of the total cross section. How can we characterize the majority of the remaining inelastic cross section? The transverse momenta are small, of the same size as that characteristic of elastic and diffractive processes, $q_\perp \sim 500$ MeV. Thus most particles are produced in soft processes for which QCD does not provide a perturbative theory. So you are forced to describe these final states using purely phenomenological techniques.

First we define some kinematics; the rapidity variable, y, is defined in Eq. A.9. Rapidity is the relativistic analogue of velocity in the sense that, for successive Lorentz transformations, rapidities add just as velocities add in Galilean transformations.

$$\sinh y = P_{11}/M_\perp \qquad \text{A.9}$$
$$M_\perp^2 = P_\perp^2 + M^2$$

The relationship between the previously defined x variable and the rapidity is given in Eq. A.10.

$$x = 2M_{\perp}\sinh(y)/\sqrt{s}$$

$$y = \frac{1}{2}\ln\left[\frac{E + P_{11}}{E - P_{11}}\right] \qquad \text{A.10}$$

In the approximation that the transverse momentum of the particle is much greater than its rest mass, and that the particle is relativistic, there is a very simple relationship between the rapidity and the polar angle, θ, of the particle. It is called the pseudo rapidity and is defined in Eq. A.11.

$$y \simeq -\ln[\tan(\theta/2)] = \eta \qquad \text{A.11}$$

As a numerical example, for a 1000-GeV proton-beam momentum the center-of-mass rapidity of the beam is ±7.7 and an object of mass 100 GeV would occur at a reduced maximum rapidity of ±3.

How are cross sections defined in a Lorentz invariant way? The Lorentz invariant one particle phase space (that means the behavior of a single particle in the absence of any dynamics and any exterior energy and momentum constraints) is given in Eq. A.12. This equation says all 4 momenta are equally probable as long as the particle is on the mass shell.

$$\begin{aligned} d^4P\ \delta(P^2-M^2) &= d\vec{P}/E \\ &= dP_{\perp}^{\ 2}dP_{11}/E \\ &= dP_{\perp}^{\ 2}dy \end{aligned} \qquad \text{A.12}$$

Mean multiplicity

In an explicitly Lorentz invariant way, this four dimensional volume element is just proportional to $dydP_\perp^2$. If the transverse momentum is dynamically cut off in some way (specified by a finite temperature) so that $p_\perp$ is limited, then the problem of phase space becomes a one dimensional problem. We can then expect that particles are produced uniformly in rapidity out to a maximum value of that variable. This means that we expect to have a "rapidity plateau" form at high energies. On that plateau, particle production would be uniform in rapidity with a particle density ρ which is constant. We can think of the particles at the end of the rapidity plateau as the fragments of either the target or the beam projectile while the central region is new particle production, i.e., thermodynamic boil off of new particles. In the asymptotic approximation that the fragments are ignored, the mean multiplicity is just the density of particles on the rapidity plateau times the maximum range of rapidity. This formula is shown in Eq. A.13.

$$\langle n \rangle \sim \left(\frac{1}{\sigma_I} \frac{d\sigma_I}{dy} \right) (2y_{max}) \qquad \text{A.13}$$
$$\sim \rho \, (2y_{max})$$

This being the case, the mean multiplicity should scale logarithmically (see Eq. A.10) with the center-of-mass energy s. Data on proton-proton collisions shown in Fig. A.6 indicate that this logarithmic scaling of the multiplicity is consistent with the data. In fact, you can think of the constant term in Fig. A.6 as being due to the beam and target fragments and the linear term [proportional to ln(s)], as being due to the expansion of the rapidity plateau as the energy increases. Of course reality is not as simple as this. The density ρ is in fact not constant. It rises roughly from a density of two charged particles to about three particles from the ISR to the CERN SPS energy regimes. At TeV I, if this trend continues, you'll have a density of five per unit of rapidity or about 30 charged tracks within ±3

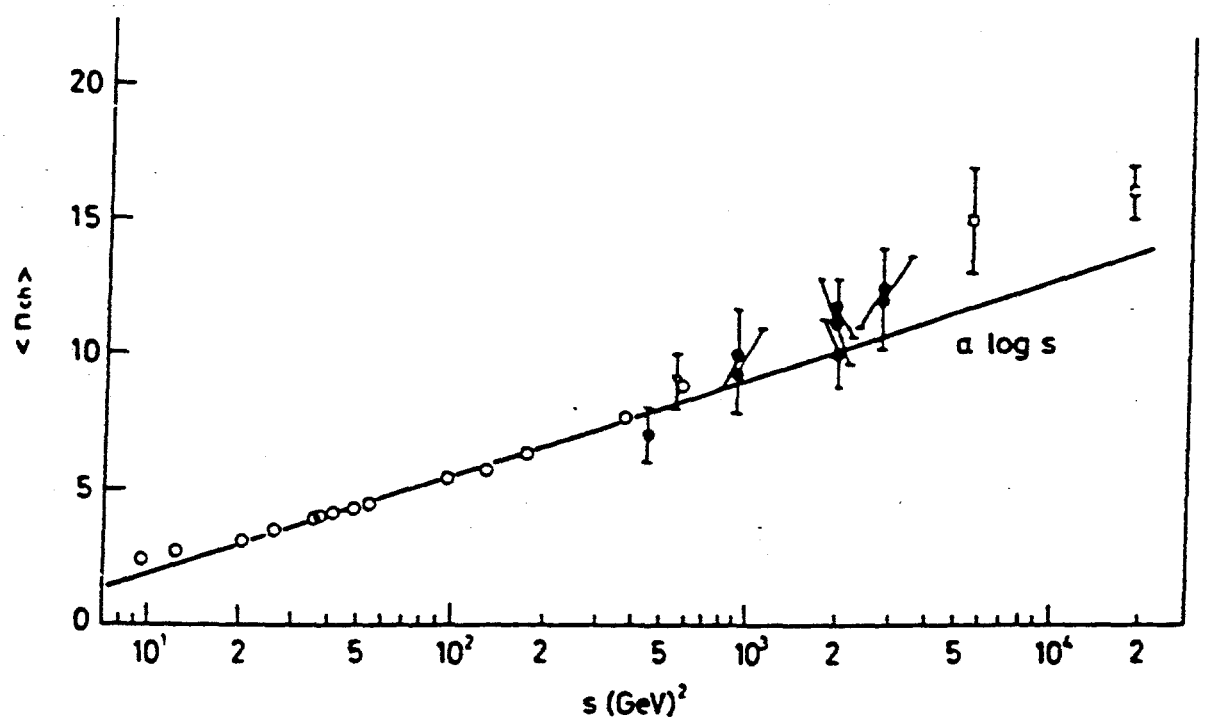

A.6 Mean charged multiplicity in pp collisions as a function of s.

units of rapidity; this is equivalent to angles greater than 5.7 degrees in the center of mass. There also appears to be a rise in the mean hadron temperature (the average transverse momentum) with s. The data from UA1 seem to indicate a mean transverse momentum of about 500 MeV. However, this is ambiguous with respect to the definition of the event sample. There are ambiguities in whether one includes jets or not, and how one defines jets. We conclude that this is indeed "soft" or ln(s) physics.

It should be remembered that in the soft collisions of ln(s) physics, the final state flavor is very important. To first order, one can consider all secondaries as being pions; the π/K ratio is about 10/1 and the $K/\bar{p}$ ratio is about 3/1. A convenient way to remember this fact (which has some motivation in the context of thermodynamic models) is to assume that all particle species are produced with equally probability but that the physical variable is $M_\perp$ and not $P_\perp$. Particle production has a Boltzmann-like weight, $\exp(-2M_\perp/kT)$ with $kT \sim 500$ MeV. For example, π/p is then $\sim\exp(+2M_K/kT) \sim 7.4$. However, at high $P_\perp$ ($P_\perp > M$), all particles are produced equally ($M_\perp \rightarrow P_\perp$).

KNO scaling

There is a curious phenomena called KNO scaling. This scaling obtains if you plot the probability for a particular produced particle multiplicity "n" times the mean particle multiplicity for all collisions at a fixed energy, as a function of the multiplicity normalized to the mean multiplicity. This is a universal function of that ratio. Data plotted in this way are shown in Fig. A.7 and the corresponding scaling Eq. A.14 is given below.

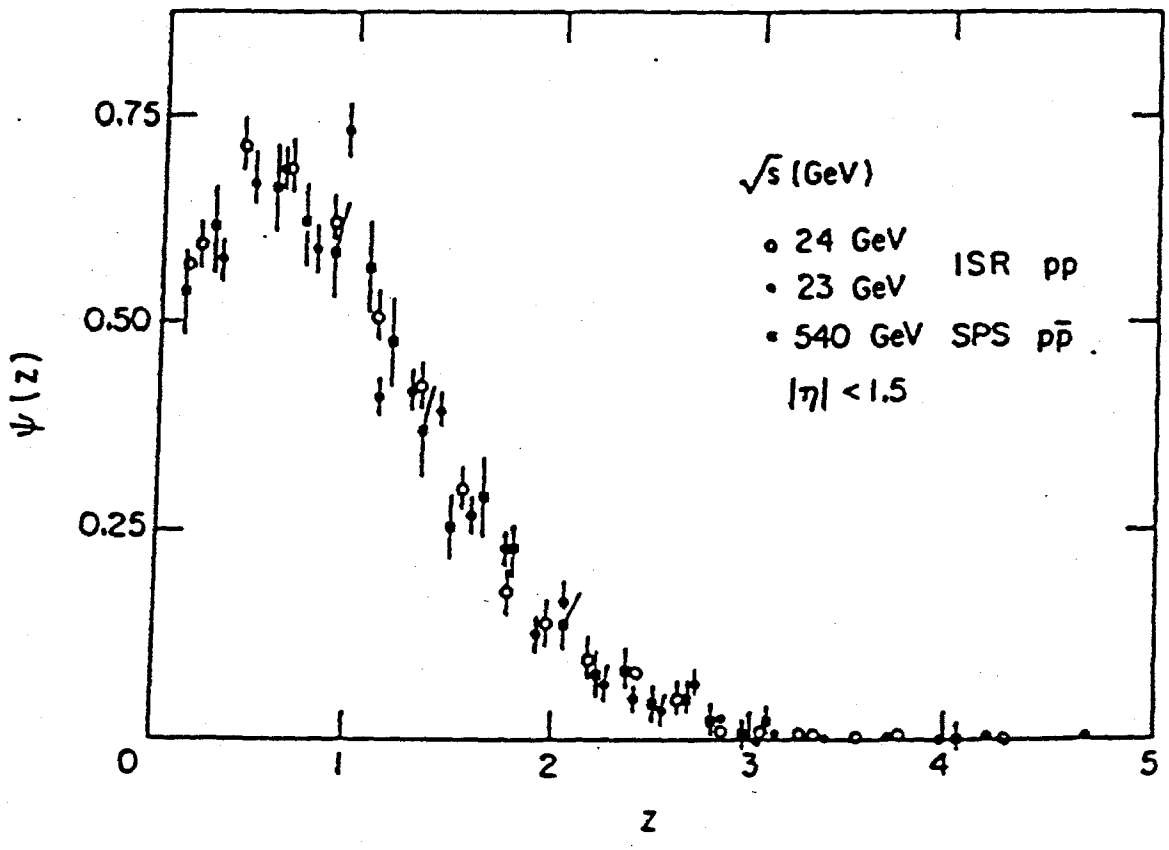

A.7 KNO scaling from ISR to CERN SPS Collider energies.

$$\langle n\rangle\ \sigma_n/\sigma_I = f(n/\langle n\rangle)$$
$$\langle n\rangle\ P_n = f(z) = \psi(z) \qquad \text{A.14}$$
$$z = n/\langle n\rangle$$

At first blush, the scaling behavior persists from ISR to SPS energies. However, the validity of the scaling depends upon your definition of the event sample (whether or not you include jets) and again it is a question of judgment.

Soft and hard scattering domains

What is the phase space region where ln(s) physics is dominant? If we define a particle density ρ in rapidity as in Eq. A.13, then the doubly differential cross section (which is proportional to the Lorentz invariant cross section) for single particle inclusive production is as given in Eq. A.15.

$$\frac{d^2\sigma}{dydP_\perp^2} \sim \frac{\rho\sigma}{\langle p_\perp\rangle^2} e^{-2p_\perp/\langle p_\perp\rangle} \sim \frac{1200\text{mb}}{\text{GeV}^2} e^{-4p_\perp} \qquad \text{A.15}$$

The cross section is about 10 microbarns/GeV^2 at a transverse momentum of 5 GeV which is 10 times the average transverse momentum for soft processes. At this value of transverse momentum, hard scattering processes begin to dominate. They are characterized by power law behavior of the differential cross section as a function of $p_\perp$ rather than the exponential behavior characteristic of soft ln(s) physics. We can consider this value of $p_\perp$ to mark a transition between ln(s) physics and the regime of hard scattering, where we feel we have a fundamental theory for the processes which are occurring. The cross section above this $p_\perp$ is roughly 10

microbarns, which is ~ 1/1000 of the inelastic cross section. This means that the processes for which we feel we have some fundamental theory and some deep understanding are in fact very rare hadronic processes.

Phase transitions/gluon plasma

The theory we do have for hadronic interactions, which is quantum chromodynamics (QCD) is a theory which at high temperatures exhibits a phase transition. This phase transition is the analogue of ionization. Lattice gauge calculations tell us that the phase transition is inevitable. At zero temperature, the quarks are permanently confined and are frozen in; at elevated temperatures, asymptotic freedom and color screening tell us that we expect a deconfined quark gluon plasma to be formed. There is a phase diagram which indicates that, if one can raise the temperature of hadronic matter beyond a critical point, this quark gluon plasma phase will occur.

In the context of the lattice gauge calculations, the transition temperature at which this phase transition is supposed to occur is of the order of a few Λ (on the same scale as the average transverse momentum in soft ln(s) processes). Unfortunately, it is not clear how the formation of this plasma manifests itself. Is it indicated by a transition to high multiplicities? Is it indicated by the sudden appearance of statistically equal production of light and heavy quark flavors? That the latter effect could occur arises from the fact that the gluons of QCD (which are the strong force carriers) are flavor blind. Their couplings to quarks are flavor independent. We, therefore, might expect democratic production of heavy flavors. This phase transition should not be a particularly rare process when one has elevated the colliding-beams energy or the complexity of the projectile and target sufficiently to form an adequately elevated temperature.

The TeV-I experiment to study this phenomenon is E-735 which is in intersection region CØ. It's basically a low-luminosity experiment and that implies that the cross sections that they will be able to look at will be ones that occur at substantial levels. Basically they will look at multiplicities and heavy flavors (in particular kaons), and search for the formation of a quark-gluon plasma. The layout for E-735 is shown in Fig. A.8.

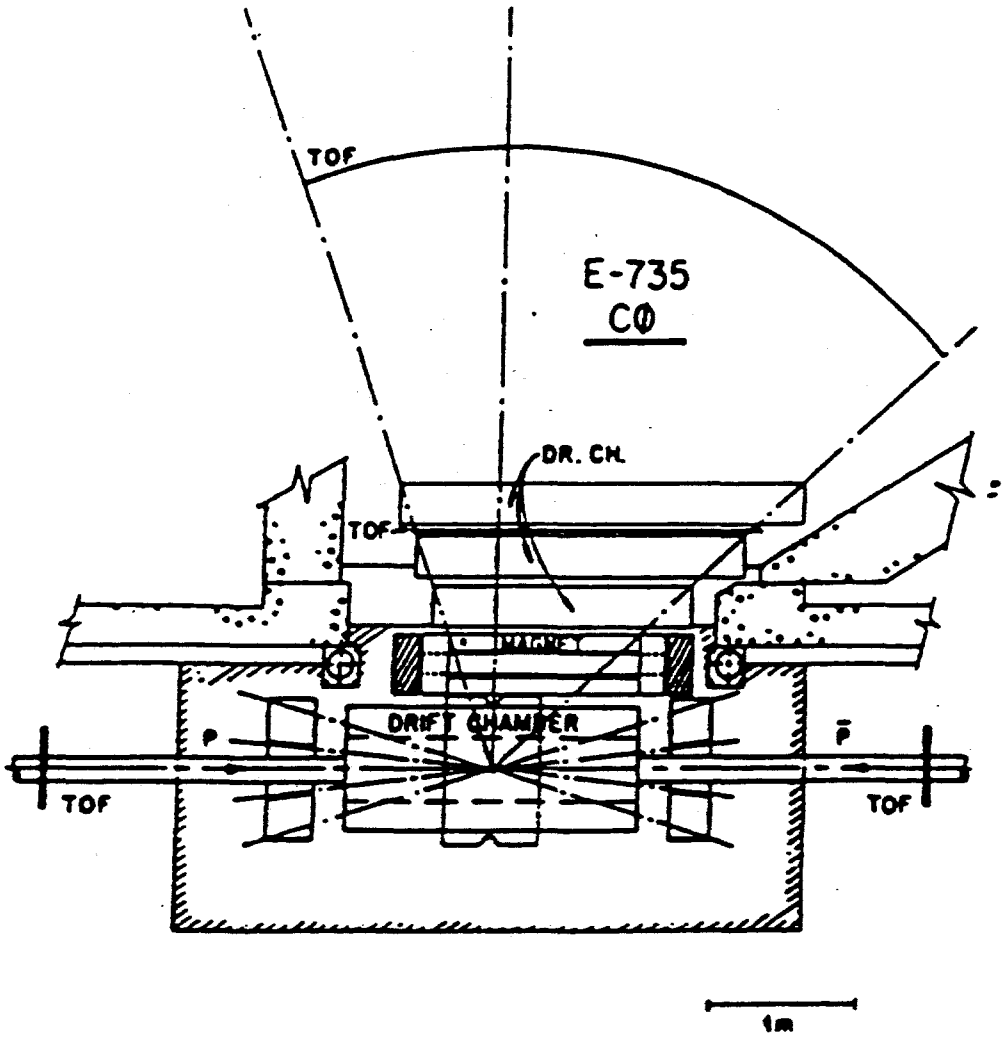

A.8 Layout of E-735 (CØ).

B. Hard Scattering and Hadron Jets.

Partons and kinematics

One of the major advances in high-energy physics in the last 20 years was the realization that hadrons (such as the proton) consist of a bound collection of point like partons. The partons are quarks and gluons (the quantum force carriers of QCD). How do we find out how the partons are distributed in a proton? In principle QCD would allow us to solve the problem from first principles like the hydrogen atom. In practice the problem is non-perturbative and we resort to measurement. We look at the proton by shining a light on it (really, you scatter leptons inelastically from the proton). If you look at Fig. B.1, you'll see that momentum and energy conservation means that, if you measure the incoming and outgoing lepton, you know everything about the "virtual" photon which is shined on the proton. Elastic scattering can be characterized by only one Lorentz invariant, the four-momentum transfer. In the inelastic case we have two invariants to choose from, the four-momentum transfer to the proton and the mass of the final-state system. In fact, in Eq. B.1, we define two other invariants which are q^2 (the mass^2 of the exchanged photon) and $\underline{P}.q$ which is the second invariant. We define x to be the ratio of q^2 to $\underline{P}.q$. Note that this is not the x which we used in Section A.

$$x = -q^2/2\underline{P}.q \qquad \text{B.1}$$

Bj had the fundamental revelation that (in a certain kinematic regime) measuring x is accomplished directly by measuring incoming and outgoing leptons; this, in turn, allows you to measure the momentum fraction of the proton carried by the constituent off of which the scattering occurs. This basic kinematic fact is seen by reference to Fig. B.1 and to Eq. B.2 which defines the kinematic variables. A parton with

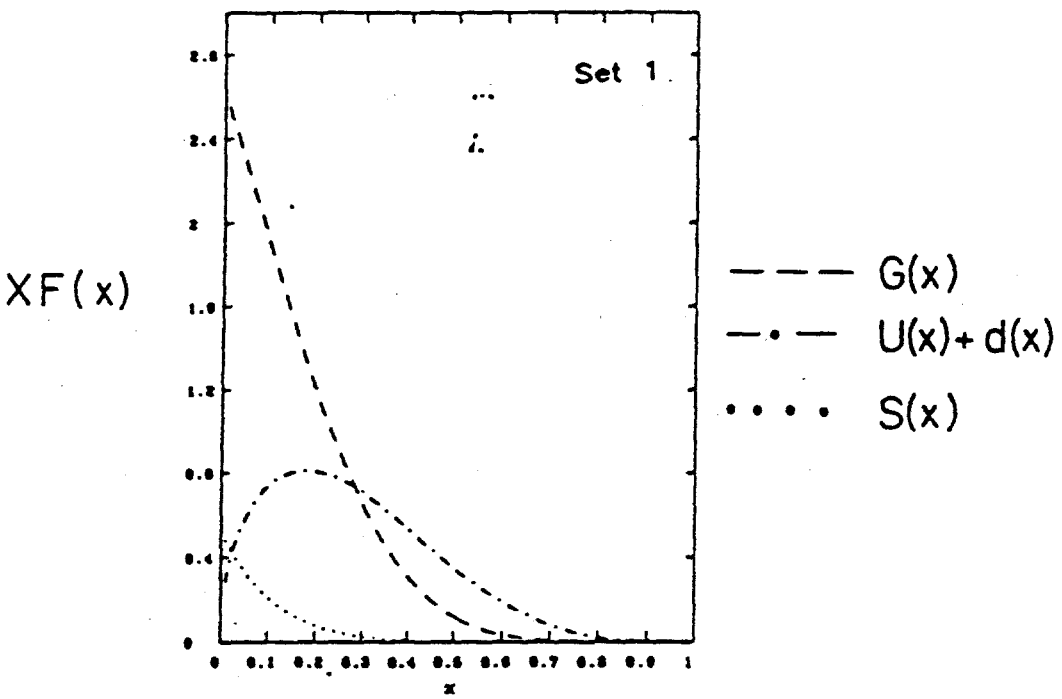

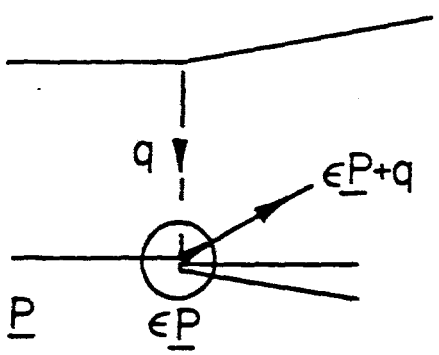

B.1 Parton distribution functions as a function of x.

momentum fraction ε of the proton momentum $\underline{P}$ scatters off the exchanged photon and exits with a momentum $\varepsilon\underline{P}+q$.

$$(\varepsilon\underline{P} + q)^2 - m_q^{\ 2} = 0$$

$$\varepsilon^2 M^2 + q^2 + 2\varepsilon\underline{P}.q - m_q^{\ 2} = 0 \qquad \text{B.2}$$

If we look in a regime where q^2 gets very large and simultaneously $\underline{P}.q$ gets very large, that means that all intrinsic mass scales are irrelevant. In this regime where the proton mass (M) and the quark mass (m_q) are vanishingly small it is easy to see as in Eq. B.3 that x is indeed equal to ε.

$$q^2 + 2\varepsilon\underline{P}.q \simeq 0 \qquad \text{B.3}$$

$$\varepsilon \simeq x$$

Remember that x is measured by measuring only the ingoing and outgoing leptons; they tag the exchanged photon. ε is the fraction of momentum carried by the parton which was struck by that photon. By performing such a set of experiments, one can measure the distribution function for partons within the proton.

A compilation of the results of many such experiments is given in Fig. B.1. If we were dealing with a non-relativistic weakly-bound system like the hydrogen atom, binding and internal parton motion would not be important on the scale of rest masses. You would further expect that for three consitutents, each one would carry 1/3 of the proton's momentum (x = 1/3). The constituents would have no high velocity relative motion. In relativistic quantum field theory, binding means that you exchange quanta (gluons) and you also have bubbles of quark anti-quark pairs. That means, in turn, that the momentum distribution function for the constituents will reflect the relative motion between them. Also, there will be a distribution function of the constituents as a function of their transverse momentum and a

distribution function for internally radiated quanta such as gluons and antiquarks. Strange quarks and gluons, for example, exist in the proton as a result of radiative processes and they will have their own distribution functions. Recalling the bremsstrahlung spectrum, it's probably not surprising that they will have distribution functions that look something like 1/x. The shapes for the distribution functions are shown in Fig. B.1. In this figure, the gluon distribution function, the up and down valence quark distribution in the proton, and the sea quark distribution from $q\bar{q}$ pairs are shown separately. You can see that the gluons and sea quarks have a typical radiated shape whereas the valence quarks peak at an x of about 0.15 or 0.2 which is close to the 1/3 value that you would expect with no binding; the mean momentum is shifted downward because of momentum conservation in the radiative processes and its shape is smeared out because of these virtual processes. Notice that, if you are at an x less than 0.3, you are dominated by gluons, whereas, if you are at an x greater than 0.3, you are dominated by valence quarks.

Note that no q^2 evolution of the distribution functions is specified. In any quantum field theory the distribution function will not obey "scaling" i.e., be a function only of x, but will have "scaling violations" and depend on x and q^2, $F(x,q^2)$. This topic is treated in the references. The q^2 evolution is slow and thus (logarithmic q^2 dependence) ignored for our crude estimations.

Sum rules for partons

The distribution functions must satisfy various conservation laws. Some examples are shown in Eq. B.4. They are simple statements that the proton consists of a net of two valence up quarks and one valence down quark; that the strange quarks exist only as quark/antiquark pairs so that the net number of strange quarks is zero; and that the gluons are responsible for the binding and carry (on average) half of the momentum of the proton.

$$\int_0^1 [u(x) - \bar{u}(x)]dx = 2$$
$$\int_0^1 [d(x) - \bar{d}(x)]dx = 1 \qquad \text{B.4}$$
$$\int_0^1 [s(x) - \bar{s}(x)]dx = 0$$
$$\int_0^1 xG(x)dx \sim 1/2$$

Simple fits are made to the distribution functions. They are typically of the form shown in Eq. B.5. The strange quarks fall off very rapidly, $(1-x)^8$. The gluons fall off as $(1-x)^5$ and the valence up and down quarks have a peak at non zero values of x and fall off as $(1-x)^3$ and $(1-x)^4$ respectively.

$$xF(x) = x^{\alpha}(1-x)^{\beta}$$
$$xu(x) \sim \sqrt{x}(1-x)^3$$
$$xd(x) \sim \sqrt{x}(1-x)^4 \qquad \text{B.5}$$
$$xG(x) \sim (1-x)^5$$
$$xs(x) \sim (1-x)^8$$

Hard parton collisions

What about the kinematics of parton-parton scattering? Let us define the center-of-mass system for hadron-hadron scattering where each of the incoming hadrons has a momentum $\underline{P}_0$ and the two are oppositely directed. The total momentum of the system is zero, and the total energy is 2 $\underline{P}_0$. In the parton-parton frame (which is the subprocess) we assume that the binding process causes only very small transverse momenta which we ignore from here on. Initial state gluon bremmstrahlung is ignored. Then hadron-hadron scattering consists of parton-parton scattering where the parton from hadron one has momentum fraction x_1, the parton from hadron two has momentum fraction x_2, and they are oppositely directed. The transverse momentum in the overall center-of-mass frame is zero, by assumption, and the longitudinal momentum of

the system is $(x_1-x_2)\underline{P}_0$. As shown in Eq. B.6, x of the parton-parton system is then equal to x_1-x_2. The two partons form a system with total mass squared being the total four momentum squared which is defined to be $\hat{s}$. In general, the hat over a variable means that variable refers to the partons or subprocesses.

$$\begin{aligned} \sqrt{s} &= 2\,\underline{P}_0 \\ x &= x_1 - x_2 \\ \hat{s} &= M^2 \end{aligned} \qquad \text{B.6}$$

The relationship between s and x_1 and x_2 is easy to figure out. Square the energy which is proportional to $(x_1 + x_2)^2$. Subtract the squared momentum of the system which is proportional to $(x_1 - x_2)^2$ and you are left with the relationship that $\hat{s}$ is equal to s times x_1x_2. As seen in Eq. B.7 we define a dimensionless parameter τ which we will see over and over again. It is the ratio of the parton-parton center-of-mass energy to the hadron-hadron center-of-mass energy squared. We can take the relationships between x_1x_2 and x and τ and invert them. That relationship is also given in Eq. B.7.

$$\begin{aligned} \hat{s}/s &= \tau = M^2/s = x_1x_2 \\ x_{1,2} &= \sqrt{\tau+(x/2)^2} \pm x/2 \end{aligned} \qquad \text{B.7}$$

If we look at Eq. B.7, we can see the minimum of x_1 occurs when x_2 is equal to one. That minimum value is then τ. The average value in some sense will occur when x of the system is zero, which means x_1 and x_2 are equal to $\sqrt{\tau}$. For example, take the TeV-I collider so that P_0 is 1000 GeV. That means $\sqrt{s}$ is 2000 GeV. Consider production of 100 GeV objects. At x = 0, $x_1 = x_2 = \sqrt{\tau} = 0.05$. Looking at Fig. B.1

we know that we're probing the gluons since they dominate at these values of x. Hence, for these masses, at this $\sqrt{s}$, a pp and $\bar{p}p$ collider will be very similiar since valence quarks are not important.

The other ingredient that goes into the calculations that one does for the TeV I collider, is the cross section for the hard subprocess. For example, e^+e^- annihilation has a cross section $\hat{\sigma} = 4\pi\alpha^2/3\hat{s}$. If you put in numbers, $\hat{\sigma}$=87 nanobarns/$\hat{s}$ if $\hat{s}$ is given in GeV². For M=100 GeV, $\hat{\sigma}$ is 8.7×10^{-36} cm^2. It's easy to understand what the cross section is on dimensional grounds. We've said this kind of scattering has no intrinsic mass scale; no intrinsic mass terms. That means that if $\hat{s}$ goes to infinity, the cross section (which has the dimensions of a length squared) will have the dimensions of an inverse energy squared or a center-of-mass energy. Dimensional analysis then implies that $\hat{\sigma}$, which is the cross section for the hard-scattering process of the partons, should be just a coupling constant to the fourth power (because you have two vertices separated by a propagator) divided by $\hat{s}$. The formula for $\hat{\sigma}$ is then given in Eq. B.8.

$$\hat{\sigma} \simeq g^4/\hat{s} \qquad \text{B.8}$$

You can look at Rutherford scattering to convince yourself that this form is appropriate. As an example, in Eq. B.9 $(\hbar c)^2$ is 0.4 GeV^2 millibarns. If we take the coupling constant squared to be typical for a strong QCD like process we have α_s, the strong coupling constant, to be 0.1. If we consider the subprocess to occur at a mass of 100 GeV, then $\hat{\sigma}$ is 0.4 nanobarns. We'll see that this is the typical size for a cross section for 100-GeV objects being produced hadronically at the TeV-I collider. By comparison, electromagnetic production is down by $\sim (\alpha/\alpha_s)^2$.

$$(\hbar c)^2 = 0.4 \text{ GeV}^2 \text{ mb}$$
$$g^2 = \alpha_s = 0.1 \qquad \text{B.9}$$
$$M = 100 \text{ GeV} = \sqrt{\hat{s}}$$
$$\hat{\sigma} = 0.4 \text{ nb}$$

Hard hadron collisions

We now have the two ingredients which we need to calculate hadron-hadron hard-scattering processes. We have the parton distribution functions and we know the hard-scattering subprocess cross section. There is a comprehensive reference for such hard processes called EHLQ (Ref. B.1) in which is calculated all of these processes exactly. It should be considered the standard reference. Looking at Fig. B.2 we have composite particle A colliding with composite particle B at a center-of-mass energy squared of s. We know that composite particle A has a distribution of parton momenta $F(x_1)$ and composite particle B has a distribution $F(x_2)$. Two partons interact at two vertices with an intermediate field (gluon or other gauge particle), forming a system with longitudinal-momentum fraction x and subenergy $\hat{s}$. The simplest process has two vertices and we expect that the cross section will go like g^4.

For simplicity let's assume initially that the subprocess forms a system of fixed-mass M with a narrow decay width Γ. Then as seen in Eq. B.10, the cross section $d\sigma/dx$ is just the joint probability of x_1 and x_2 integrated over the two source distribution functions with the kinematic constraints which we have already worked out. We require x_1 and x_2 to be such that we have the relationship between s and $\hat{s}$ and that x_1 and x_2 form the system with total value equal to x.

$$\frac{d\sigma}{dx} = \frac{8\pi^2\Gamma}{M} \iint dx_1 dx_2 F(x_1)F(x_2) \qquad \text{B.10}$$
$$\delta(x_1 x_2 s - M^2)\delta(x_1 - x_2 - x)$$

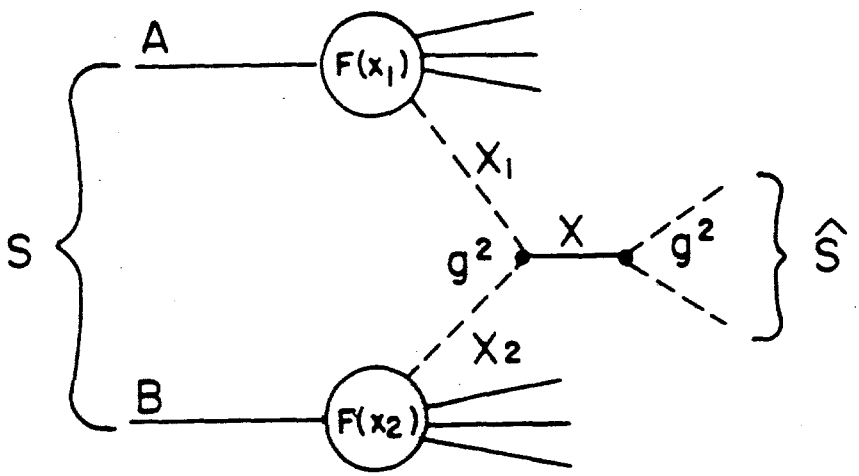

B.2 pp scattering and parton-parton scattering.

It's fairly easy to do the two delta functions. The result that you get is shown in Eq. B.11. We'll have use of this equation several times in what follows. Note the characteristic $1/M^3$ behavior, and that σ is proportional to Γ.

$$\frac{d\sigma}{dx} = \frac{8\pi^2\Gamma}{M^3}\left[\frac{x_1F(x_1)x_2F(x_2)}{x_1 + x_2}\right] \qquad \text{B.11}$$

s-dependence in hard scattering

Using Eq. A.10, we can relate x and y and find the differential cross section as a function of y. Specializing to the case where the system is produced at rest in the center of mass, we find $d\sigma/dy$ at y=0 as given in Eq. B.12.

$$\left(\frac{d\sigma}{dy}\right)_{y=0} = \frac{8\pi^2\Gamma}{Ms}\left[F^2(\sqrt{\tau})\right] \qquad \text{B.12}$$

As an example one can take this expression and use the gluon structure functions that we defined previously. If the gluon distribution function is normalized so that half of the hadron momentum is carried by the gluons, then we get a form for G(x) given in Eq. B.13.

$$G(x) = 3(1-x)^5/x \qquad \text{B.13}$$

$$\frac{M^3}{\Gamma}\left(\frac{d\sigma}{dy}\right)_{y=0} = 9\pi^2(1-\sqrt{\tau})^{10}$$

We have inserted a factor required by color counting. There are eight gluons from the proton, and eight gluons from the antiproton. There are 64 possible combinations, only eight of which are colorless. We require that the outgoing hadron

of mass M be colorless. That gives us a reduction factor of eight. The resulting prediction for gluon-gluon production of a system of mass M is given in Eq. B.13. The first thing to notice is that $M^3/\Gamma\ (d\sigma/dy)_{y=0}$ should be a function of the scaling variable τ only. Fig. B.3 shows a compilation of data on pp production of vector mesons. Indeed, this scaling works fairly well. A more specialized prediction is that if the gluon structure functions go like $(1 - x)^5$ then we have a sharp threshold behavior due to the "radiative" nature of the gluon source function in τ, which goes like $(1 - \sqrt{\tau})^{10}$. That curve is also shown in Fig. B.3 and seems to represent the threshold behavior of the data unreasonably well. As a rule of thumb, for $\sqrt{\tau} < 0.1$ no large gain in σ with increasing s is obtained.

Total cross sections for hard scattering.

The total cross section for the hard process can be found by integrating Eq. B.11 over all x values. The limits on x_1 are from τ to 1. Recall that τ is the minimum x value (at a given mass) that can be probed. Dimensional arguments say that the width is proportional to the coupling constant squared times the only mass scale that is available which is M. The resulting formula for the total cross section is given in Eq. B.14.

$$\sigma \sim \frac{\Gamma\tau}{M^3} \int_\tau^1 \frac{dx_1 F(x_1) F(\tau/x_1)}{x_1} \qquad \text{B.14}$$

$$\Gamma \sim g^2 M$$

Using the functional dependence assumed for the quark and gluon distributions, this integral has no particular simple closed form and needs to be done numerically. These kinds of consideration lead the authors of EHLQ to define a differential luminosity for the process as given in Eq. B.15.

$$\frac{d\sigma}{d\tau} \sim \hat{\sigma}(dL_{ij}/d\tau) \qquad \text{B.15}$$

$$\frac{dL_{ij}}{d\tau} \quad \int_\tau^1 \left[\frac{dx F_i(x) F_j(\tau/x)}{x} \right]$$

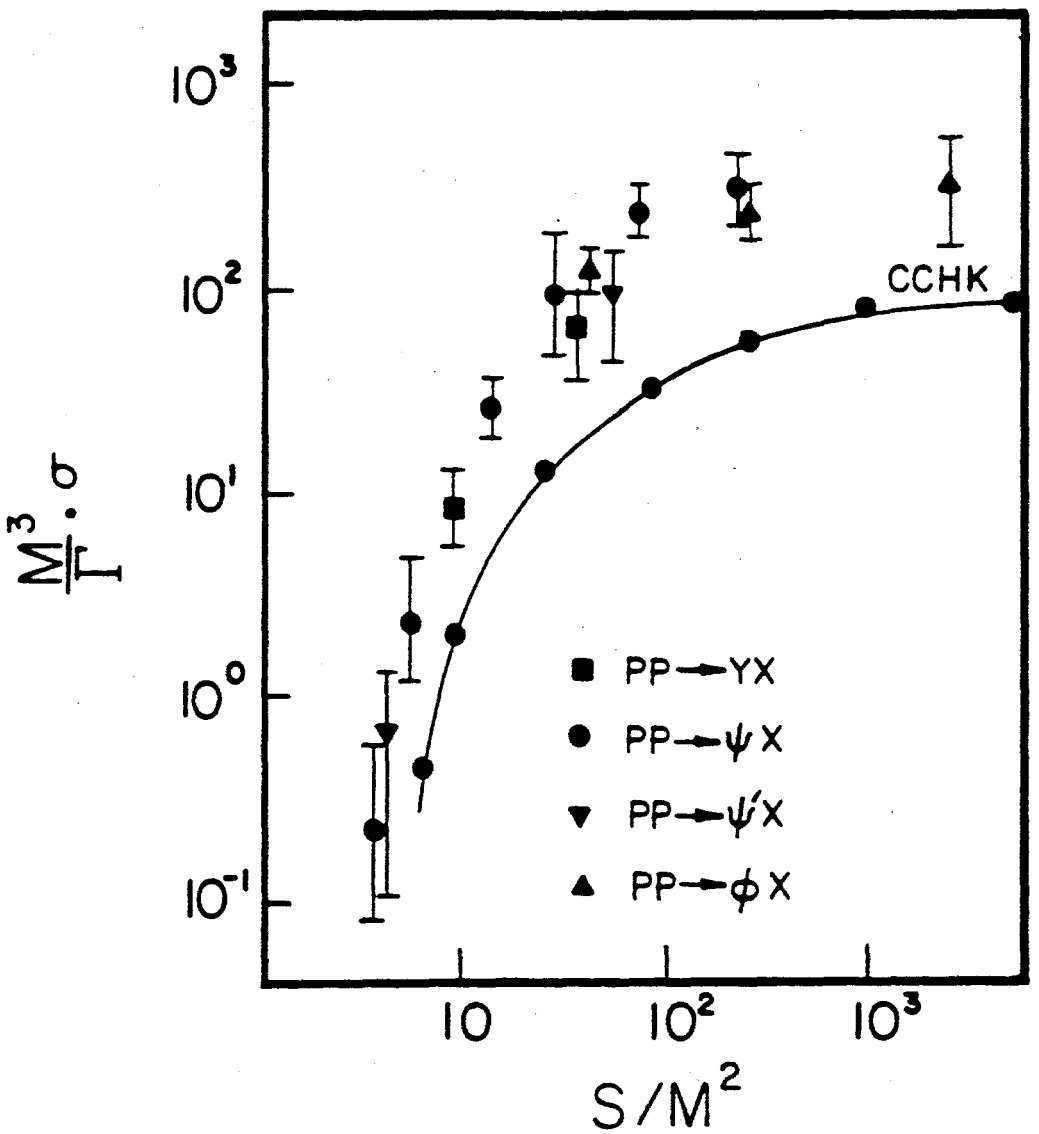

B.3 Cross section for pp production of vector mesons; scaling of $M^3/\Gamma\,\sigma$ as a function of $1/\tau$.

Comparing Eqs. B.14 and B.15, it is easy to see that the cross section in hadron/hadron scattering is proportional to this differential luminosity. The proportionality is given in Eq. B.16.

$$\sigma(\tau) \quad g^4\left(\frac{\tau}{M^2}\frac{dL}{d\tau}\right) . \qquad \text{B.16}$$

Note (using Eq. B.8) that $\sigma(\tau) \sim \hat{\sigma}(\tau\, dL/d\tau)$.

Using the quark and gluon distribution functions, we can work out the differential luminosity for any process of interest, for example gluon-gluon fusion, $u\bar{u}$ annihilation in proton/antiproton scattering, and processes of this sort. As was previously stated, these integrals don't have any particular simple closed form. The gluon-gluon differential luminosity as numerically evaluated in the regime of masses M between 20 and 400 GeV at a center-of-mass energy $\sqrt{s}$ = 2000 GeV is well represented by the power law given in Eq. B.17.

$$\frac{\tau}{M^2}\left(\frac{dL_{gg}}{d\tau}\right) \sim 10^7 \mu b/[M(GeV)]^{3.5} \quad . \qquad \text{B.17}$$

Note that the mass dependence $1/M^{3.5}$ will occur in all our discussions of hard scattering processes. Using this parameterization of the gluon-gluon luminosity, plugging into Eq. B.16, we can evaluate the cross section for producing a 100 GeV mass system. For a strong process we have $g^4=(\alpha_s)^2$. The result is a cross section of 10 nanobarns. You remember that the hard subprocess cross section was 0.4 nanobarns. This is a reflection of the large gluon flux available for "light" particles (with $\hat{s}/s=\tau<<1$).

$$M = 100 \text{ GeV}, \; g^4 = \alpha_s^{\;2} \qquad \text{B.18}$$
$$\sigma \sim 10 \text{ nb}, \; \hat{\sigma} = 0.4 \text{ nb} \quad .$$

Heavy quark pair production

Finally we are ready to calculate the production cross section for heavy quark pairs at the TeV-I collider. The idea is that gluons are flavor blind. That means, in particular, that for hard processes in strong interactions, flavor is much less important than it is in soft processes. You remember that in soft processes, pions were produced an order of magnitude more copiously than kaons. In the case of hard processes, flavor-blind glue is the most likely mechanism for heavy-flavor production. This goes under the catch phrase of gluon-fusion production. The exact predicted cross section for heavy-flavor production at the Tevatron collider is shown in Fig. B.4. A rough estimate that we now know how to make is given in Eq. B.19.

$$\sigma_{Q\bar{Q}} \sim \alpha_s^2 \left(\frac{\tau}{M^2} \frac{dL_{gg}}{d\tau} \right)_{M=2M_Q} \quad . \qquad \text{B.19}$$

The subprocesses is also shown in Fig. B.4; it is gluon-gluon fusion from the proton/antiproton forming a quark-antiquark pair at low relative momenta. The mass of the pair is then roughly equal to the sum of the masses of the quarks. For example taking a strong coupling constant α_s of 0.1, a b quark of 5 GeV gives us a $b\bar{b}$ mass of 10 GeV. These assumptions lead us to predict a cross section for $b\bar{b}$ pair production of 30 microbarns. As can be seen from the Figure the exact prediction is 25 microbarns. You can also see from the Figure the characteristic power law fall off for hard processes, (it is a log-log plot). You expect a power law to be a straight line. In fact, $1/(M)^{3.5}$ is a reasonable fit to this Figure. Obviously Figs. B.3 and B.4 are related in some fashion. In Fig. B.3 we were looking at gluon-gluon fusion into a vector mesons which you can think of as a hidden heavy-flavor state. As you recall, the scaling law is $1/M^3$. For $Q\bar{Q}$ pairs it is again gluon-gluon

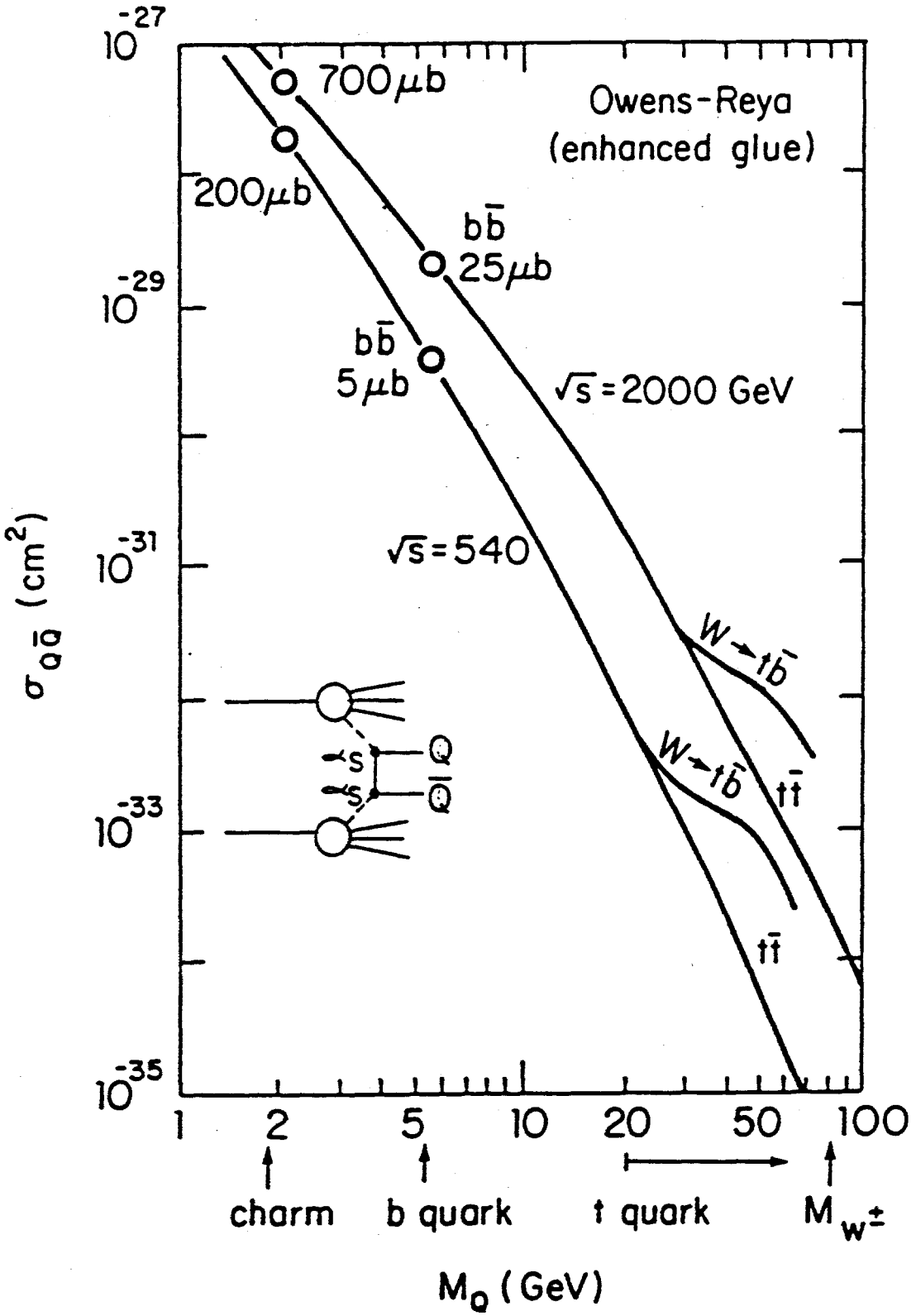

B.4 Cross section for heavy quark production at the TeV-I collider as a function of the quark mass.

fusion but the Q and $\bar{Q}$ do not stick together into a narrow state. Again the scaling is an inverse power law, something like $1/M^3$. Note (Figure B.4) that for "light" Q such as charm there is little advantage to increased $\sqrt{s}$, while for heavy Q (i.e., $\sqrt{\tau} \gtrsim 0.1$) there is a large advantage to the TeV-I collider. This fact is now easily understood.

Supersymmetry and lepton production

Just as a comment, for any other sort of gluon-gluon process if you know the coupling constant you can predict the cross section. For example, in supersymmetry every quark and lepton fermion has a scalar superpartner, and every vector boson such as the W,Z, gluons, and photons will have a fermion superpartner. The coupling constants for these partners are known from the symmetry. For example, the gluino couplings are known from the gluon coupling. Gluon + gluon production of gluino pairs is related to gluon-gluon scattering. This means that (exactly as we've done above) you can predict what the cross section for your favorite gluino-pair mass would be.

There is a situation in the TeV-I collider which is rather different from TeV-II fixed-target operation. The production rate of high transverse momentum leptons at the collider is not particularly small. This is related to what we've just been discussing, the copious production of heavy flavors at the TeV-I collider. Heavy quarks have a substantial probability to decay into leptons. The branching ratio for decay into muons is typically 10%. In the last section of this paper, we'll discuss how you estimate these branching ratios. Heavy quarks decay semileptonically into three-body final states. The average transverse momentum of the lepton is then of the order of 1/3 the mass of the heavy flavor. For example, a 50-GeV top quark gives rise to a muon with a transverse momentum of around 17 GeV. This value of $P_\perp$ is well beyond the soft ln(s) physics regime set by $P_\perp \lesssim 5$ GeV as discussed in Section A.

Hadron jets

We now take up the discussion of jet production. By jet production we mean that a parton from the proton and a parton from the antiproton interact in a two body subprocess where the exiting partons, in order to be confined, dress themselves up (fragment) colorlessly into well-collimated jets of secondary hadrons. The Feynman diagram for this process is given schematically in Fig. B.5. An estimate for the magnitude of the cross section for such processes is given in Eq. B.20.

$$\frac{d\sigma_{jj}}{dM} \sim \frac{\alpha_s^2}{M}\left[\frac{\tau}{M^2}\frac{dL_{gg}}{d\tau}\right]_{P_\perp \sim M/2} \qquad \text{B.20}$$

For example with $\alpha_s = 0.1$, the production of a jet of mass = 100 GeV at the Tevatron collider would be estimated to occur at the level of 0.1 nanobarns/GeV. Some data from the SPS collider is shown in Fig. B.5. What is plotted is $d\sigma/dM$ as a function of M and $d\sigma/dp_\perp$ as a function of $p_\perp$. The basic power law behavior of the process is again evident as is the nanobarn cross section level for the process. The estimate of 0.1 nanobarn per GeV at 100-GeV jet-jet mass is a bit low. Two body kinematics means that, on the average, you can take the jet-jet mass M and divide by two to get the transverse momentum of one of the two jets. In fact a glance at Fig. B.5 shows that this works out fairly well. Our initial estimate of 0.1 nanobarn per GeV is within an order of magnitude, and the transposition of jet-jet mass to transverse momentum by scaling down by a factor of 2 works out rather well.

Jet fragmentation

Some additional, very simple kinematics are indicated in Fig. B.6 where one has a jet-jet mass M which fragments into two partons of transverse momentums $p_\perp$ and angle θ. Subsequently these partons dress themselves in an n-body decay where the

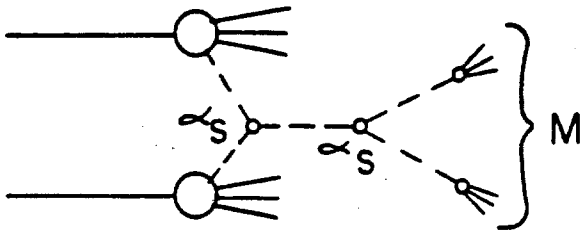

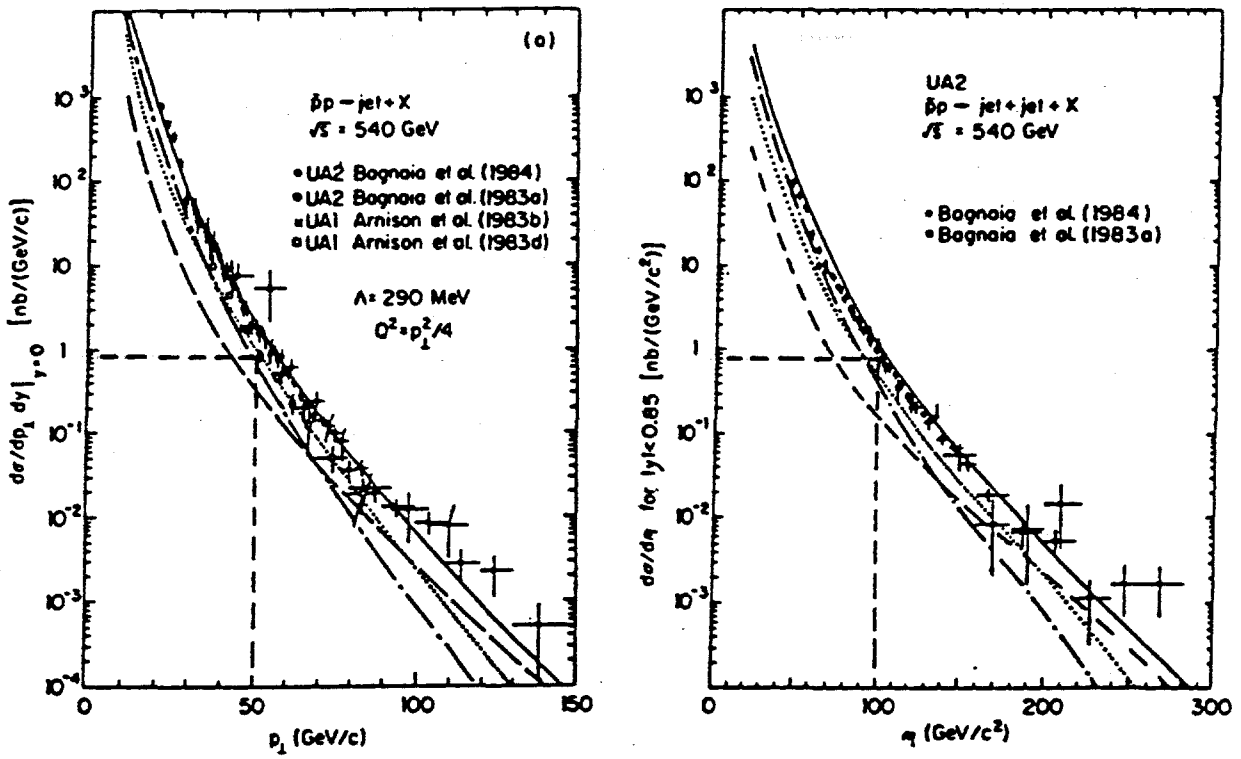

B.5 Cross section for jet production at the SPS Collider as a function of jet-jet mass, or jet $P_\perp$.

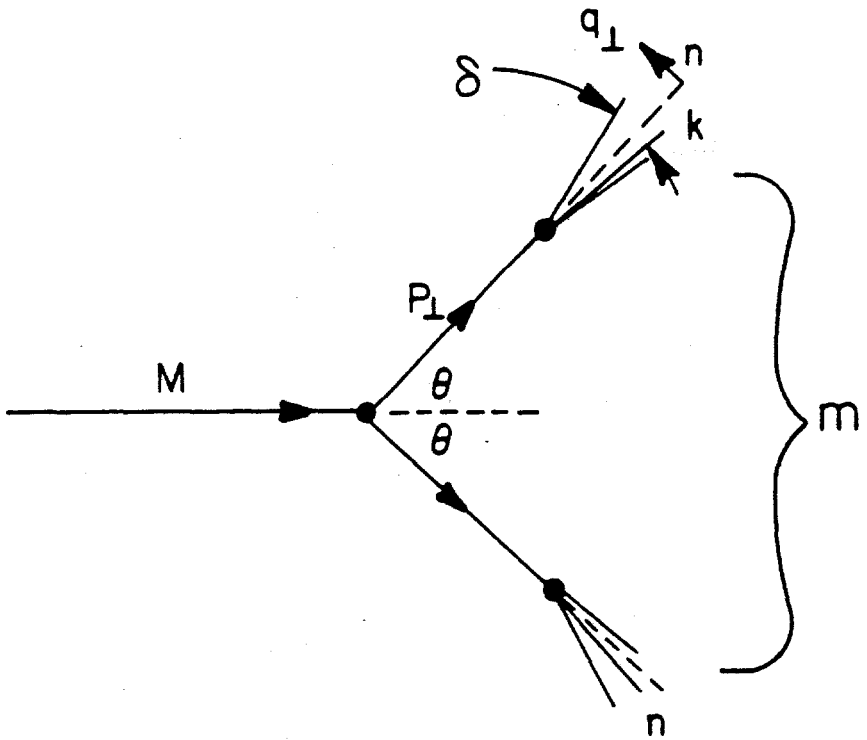

$P_\perp \sim M/2$

$k_\perp \sim P_\perp/n$

$k \sim P/n$

$m \sim M/n$

B.6 Kinematics for sequential decays.

typical momentum of the dressed hadrons is of order k. As indicated in Eq. B.21, $k_\perp$ (which is the transverse momentum of one of the hadrons from the jet) is reduced from $p_\perp$ of the jet by the multiplicity of the decay.

$$\begin{aligned} k_\perp &\sim P_\perp/n \\ k &\sim P/n \\ m &\sim M/n \end{aligned} \qquad \text{B.21}$$

If you take a fragment from one of the jets and combine it with a fragment from the other jet what is the invariant mass? The mass M is reduced by the multiplicity of the decay process to m = M/n. What is assumed in all this is that the transverse momentum of the n body fragments labelled by $q_\perp$ is small with respect to the transverse momentum direction $P_\perp$ of the initial jet (jet axis). We're assuming that the fragmentation of the jet has a limited transverse temperature (say ~ 500 MeV) very much like what we've already seen in ln(s) physics. In future we'll continue to make the assumption that the fragmentation of a jet into a number of hadrons is very much like the ln(s) physics production of secondary particles which was discussed in Section A.

This simple kinematics means that there is a relationship between the transverse momentum carried by the jet and the transverse momentum carried by the fragments of that jet (which appear inclusively as single particles at large transverse momenta). The distribution of transverse momentum of jets and of π^0 at UA2 is shown in Fig. B.7. The transposition of the jet shape at 60 GeV $p_\perp$ down to 20 GeV $k_\perp$ might be expected for a jet fragmentation into a few particles. Note that $\langle n \rangle$ varies slowly with M by appeal to Section A. More on this later. Thus we expect that the production rate of jets at a given transverse momentum is several orders of magnitude

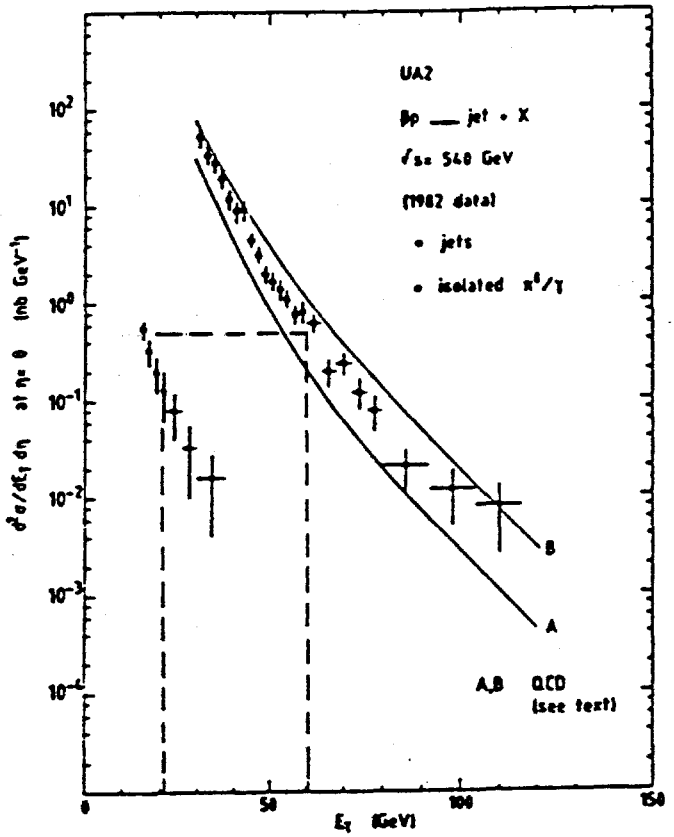

B.7 Parent/daughter, jet/π^0 cross sections as a function of $P_\perp$.

(roughly 3) higher than the production of single particles. This fact can be understood as a simple kinematic property of the decays of jets.

Luminosity reach for jets

At a luminosity of $10^{30}cm^{-2}sec^{-1}$, a continuous run for three years gives you roughly an integrated luminosity of $10^{38}cm^{-2}$. The jet-jet cross section is such that at the collider one could observe two jet events with a transverse momentum up to 700 GeV. In this context it is important to remember that different jet masses probe different x values (see Eq. B.7). At different x values one is dominated by different partons. At low x we're dominated by gluons and at large x we are dominated by valence quarks. For example, 100-GeV mass at the Collider has an average parton x of 0.05 which is in the gluon region. At 600 GeV, which is near the maximum luminosity reach of the machine, the average parton x value (approximated as $\sqrt{\tau}$) is roughly 0.3 which is in the regime where we are beginning to be dominated by valence quarks. The point here is that using different jet-jet masses we can probe different constituents within the hadrons. Moving away from jet-jet x of zero also gives us another degree of freedom to probe.

Jet scaling and parton substructure

In a more speculative vein, what we've assumed so far is that quarks are point like objects and are not composite. One possible test of this assumption is to look in jets for form-factor effects. In other words, we have assumed that $\hat{\sigma} \sim 1/\hat{s}$. If this were not the case, the shape of the jet-jet mass distribution would change. If the distribution of jet-jet masses is not as we expect, then (assuming we understand the distribution functions), we can ascribe any deviation to the composite nature of the quarks. As one might expect, the size of the composite scales that we can test at the Tevatron collider is of the order of a few TeV.

The functional form which is assumed for $\hat{\sigma}$ in jet production also has an implication for the scaling properties of jets and single particles in high $p_\perp$ processes. The form we've assumed for $\hat{\sigma}$ gives us a jet-jet mass distribution as shown in Eq. B.22a. Two body kinematics then gives us a $p_\perp$ distribution for jets given in Eq. B.22b.

$$\frac{d\sigma_{jj}}{dM} \sim \frac{\alpha_s^2}{M}\left[\frac{\tau}{M^2}\,\frac{dL}{d\tau}\right] \qquad \text{B.22a}$$

$$\frac{d\sigma}{dP_\perp} \sim \frac{\alpha_s^2}{P_\perp^3}\left[\tau\frac{dL}{d\tau}\right] = \frac{\alpha_s^2}{P_\perp^3}\,[f(\tau)] \qquad \text{B.22b}$$

The thing to note is that $P_\perp^3(d\sigma/dP_\perp)$ is a function only of the scaling variable τ. To the extent that Eq. B.21 is true, this scaling behavior should also hold for single particles since $k_\perp$ is (assuming n is a constant independent of $P_\perp$) just proportional to $p_\perp$. Hence $k_\perp^3(d\sigma/dk_\perp)$ is a function only of the scaling variable τ.

Data from the CERN SPS and the ISR collider are shown in Fig. B.8 for single particles. The invariant cross section as a function of $k_\perp$ is plotted. Remember that the invariant cross section is $d\sigma/d^4P$ (see Eq. A.12) and that's proportional to $d\sigma/dydP_\perp^2$. Thus, we expect asymptotically that $d\sigma/dP_\perp$ should scale as $(p_\perp)^{-3}$ while the invariant cross section should scale as $(p_\perp)^{-4}$. Note how the data in Figure B.8 begin with an exponential falloff ($P_\perp \lesssim 2$ GeV) which then changes into a power law falloff. Note also that the cross section at $P_\perp = 0$ is roughly s independent [ln(s) physics] while at high $P_\perp$ the s dependence is dramatic.

For comparison, you should take the soft ln(s) production cross section given in Eq. A.15 and plot this on the ISR data to see that it crosses the hard scattering data at a $p_\perp$ of about 3 GeV. We have previously mentioned this in Section A on ln(s) physics. Another point gleaned from looking at the data is that at fixed $p_\perp$ the

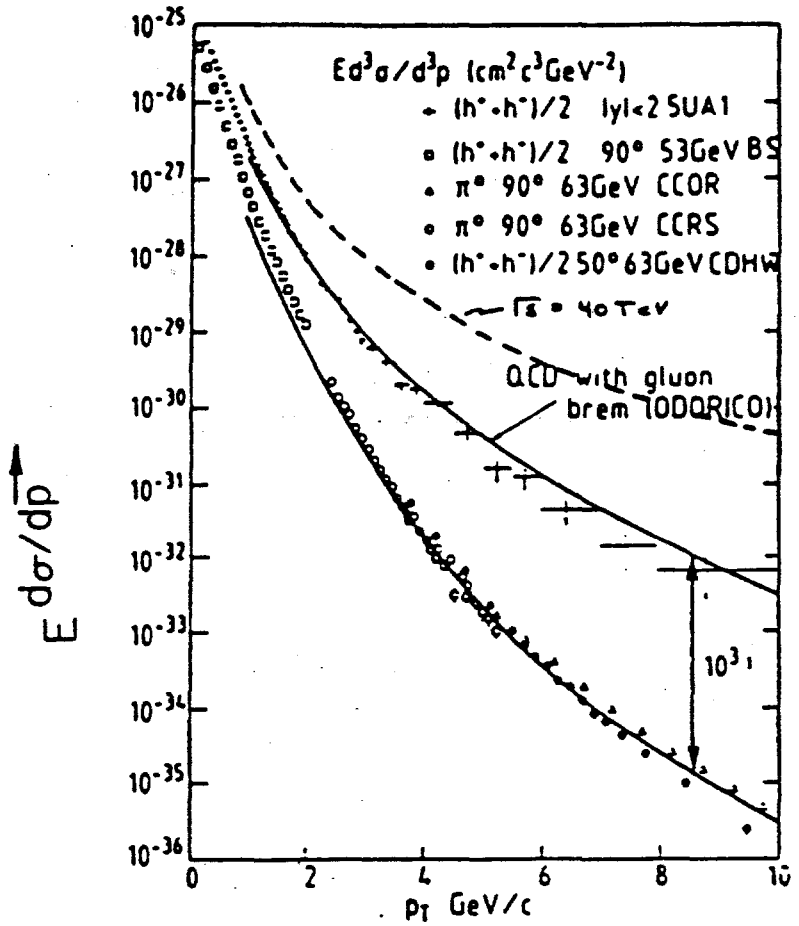

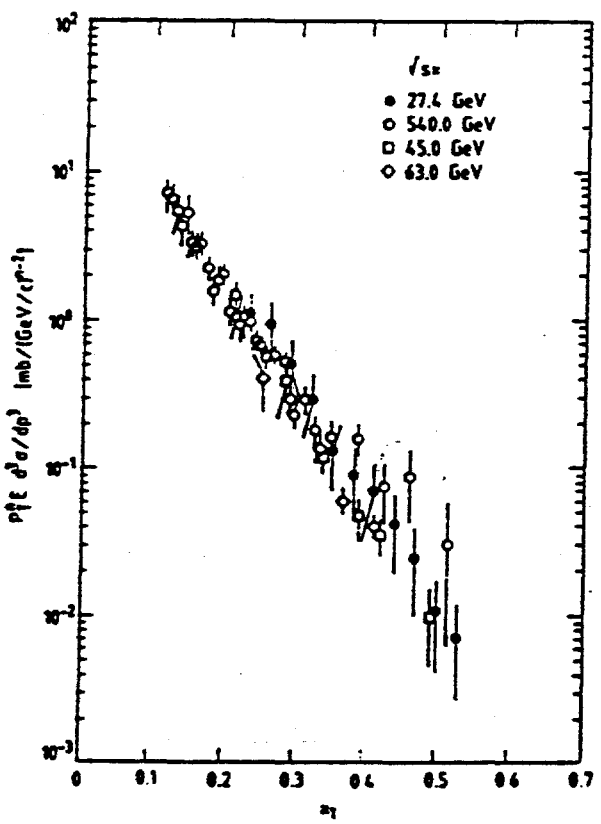

$$P_\perp^\eta \; E\frac{d\sigma}{d\vec{p}} = f(x_T)$$

$\eta = 5.1$

B.8 Scaling of jet cross sections vs $P_\perp$.

single particle cross section rises dramatically with energy. That's an indication of the scaling behavior that $p_\perp^3(d\sigma/dP_\perp)$ is a function of τ only. Also shown in Fig. B.8 is the scaling behavior of the single particle cross section from ISR to SPS energies. The vertical axis is $p_\perp^n$ times the invariant cross section as a function of $x_\perp$. The best value for n is 5.1. Recall that we expected an asymptotic scaling with a power given by four. The reason for this discrepancy is that we're not completely in the asymptotic regime yet. In fact, data spanning only the ISR-energy range initially indicated that the power was much too large, n = 8.2. Fundamentally we are not yet in a completely hard-scattering regime. There are higher twist effects, which are dying off. It's only in the regime of the SPS collider or the TeV-I collider that we are beginning to clearly uncover the true hard-scattering processes.

Jet angular distribution

If an algorithm exists to identify all the particles in a jet then we can reconstruct its total transverse momentum. Thus, up to ambiguities in identifying the jet fragments, the angular distribution of the hard scattering can be uncovered. For example, it's fairly straightforward to see that you are basically looking at a Rutherford scattering behavior. You expect $d\hat{\sigma}/d\hat{t}$ to go like 1 over the vector quantum propagator squared or $d\hat{\sigma}/d\hat{t} \sim 1/\hat{t}^2$. There's a good explanation of this fact in Ref. B.2. Some data taken from the SPS large detectors (UA1 and UA2) are shown in Fig. B.9. The vertical axis is $d\hat{\sigma}/d\cos\theta^*$, the angular distribution for jets as a function of the center-of-mass scattering angle. Simple kinematics relates $\hat{t}$ and $\cos\theta^*$ (for massless partons)

$$\hat{t} = \frac{\hat{s}}{2}(1-\cos\theta^*). \qquad \text{B.23}$$

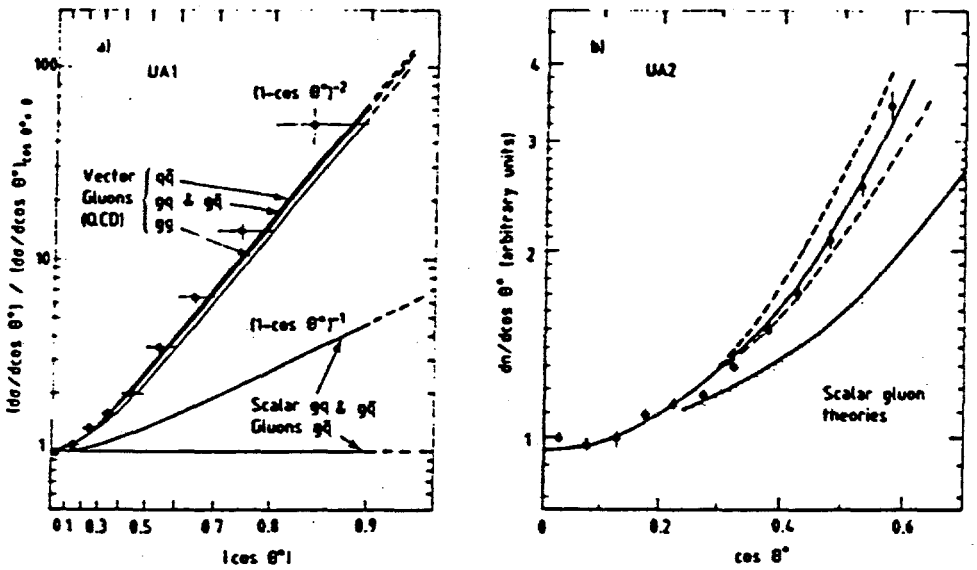

B.9 Jet angular distributions from the CERN SPS.

In particular, it looks as if a vector (as opposed to scalar) boson exchange is selected as the cause of the scattering. Fine details of the scattering dynamics are lost in our inability to define the jet fragmentation exactly. If you look at these figures, the center-of-mass angle which you can resolve, (it's a question of taste) cuts off at something like $\cos\theta^* = 0.6$ to 0.8. The reason for that, is that jets at forward and backward scattering angles mix together and are no longer distinct objects but have become collinear. In any case, the conclusion seems to be that Rutherford scattering (vector exchange) is indicated by the jet-jet data. Hence, $d\hat{\sigma}/d\hat{t}$ has the functional form given in Eq. B.24

$$\frac{d\hat{\sigma}}{d\hat{t}} \sim (g^4/\hat{s})(1/\hat{t}^2). \qquad \text{B.24}$$

Many specific parton-parton differential cross sections are compiled in EHLQ.

Observable definition of jets

Finally one has to be able to observe and define jets. It is worthwhile now to have a short discussion how they are actually observed. We recall from the discussion of ln(s) physics that if there is no dynamics then only phase space is important and it is just d^4P which is proportional to $dyd\underline{P}_\perp^2$. By analogy secondary particles from the jet fragmentation can be expected to have a uniform density in rapidity. We assume a jet (produced at 90° in the center of mass) with transverse momentum $\underline{p}_\perp$ (which is roughly the jet-jet mass M divided by 2) which fragments into particles of low mass that have a limited transverse momentum $\underline{q}_\perp$ with respect to the parent-jet direction. We also assume they are uniformly distributed in rapidity up to a maximum rapidity given in Eq. B.25.

$$
\begin{aligned}
y_{max} &\sim \ln[2P_\perp/q_\perp] \\
\delta_{1/2} &= \sqrt{2\, q_\perp/P_\perp} \\
k &\sim (e^y) q_\perp/2 \\
\delta &\sim \tan^{-1}(q_\perp/k)
\end{aligned}
\qquad \text{B.25}
$$

We conclude that the particles from the jet fragmentation are characterized by a cone with half angle which occurs at a rapidity which is $y_{max}/2$. Recall that pseudorapidity is $\ln[\tan(\theta/2)]$. That gets us the expression for the cone half angle in terms of the soft ln(s) transverse momentum $q_\perp$ and the jet transverse momentum $p_\perp$ which is given in Eq. B.25. In general, the secondary momentum k can be given in terms of the rapidity y of the fragment and $q_\perp$. Knowing k and $q_\perp$ defines the angle δ with respect to the jet axis.

Some of the kinematics for a jet mass of 200 GeV or jet-transverse momentum of 100 GeV is given in Fig. B.10. Let's assume that the soft fragmentation temperature $q_\perp$ is the same as the average value for hadronic collisions i.e, 0.5 GeV. What's shown in Fig. B.10 is the angle of the fragments with respect to the jet axis and the momentum of the secondary fragments as a function of the rapidity of the fragment. The jet half angle is 6 degrees and y_{max} is 6, so that the jet half angle occurs at a rapidity of 3. One thing that is obvious looking at this Figure is that even at 100-GeV $p_\perp$, the jet has a couple of particles which occur at rapidities of 1 and 2. They have a large angle with respect to the jet axis; 40 degrees and 100 degrees. However, they also have low momenta of order $q_\perp$ and so they are easily confused with the general ln(s) debris. Thus, it's difficult to pick up all the particles which are really in the jet because the softer fragments are lost in background debris which consists of the fragmentation of the residual constituents of the proton and antiproton.

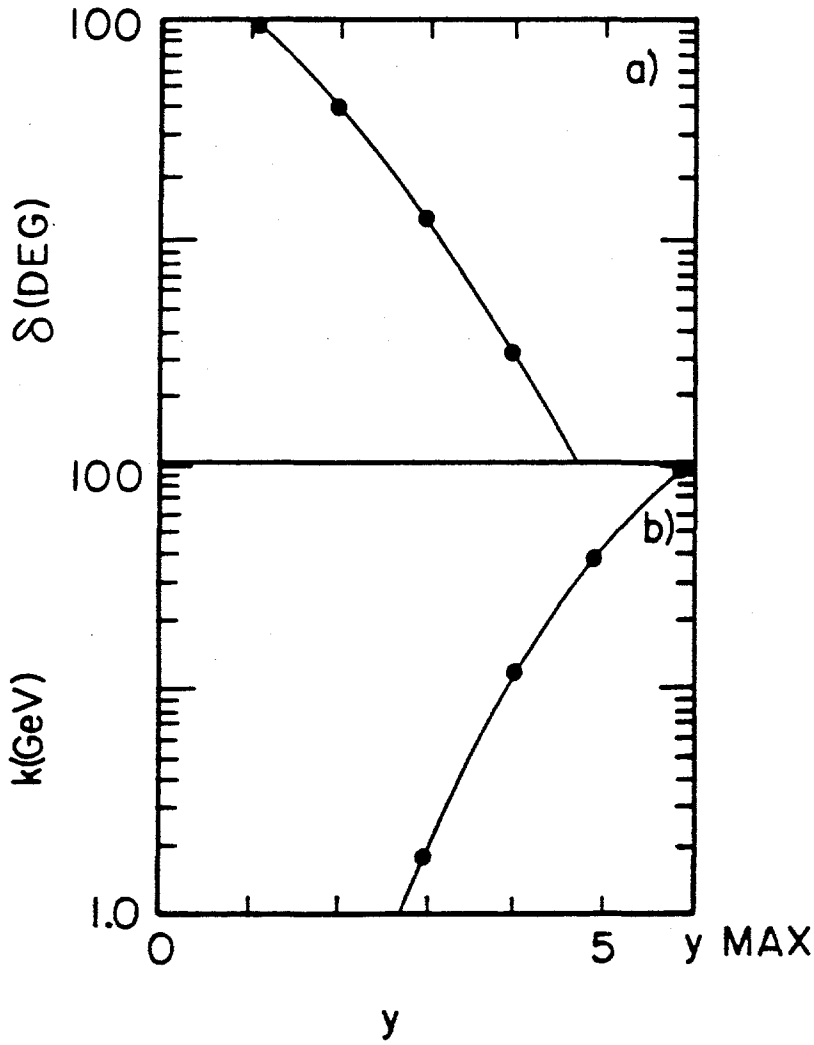

B.10 Jet framentation kinematics for a $P_\perp$ = 100 GeV jet.

Some data from an event with jet-jet transverse energy (~ M) of 200 GeV is shown in Fig. B.11. This is called a "LEGO plot". The height in this plot is proportional to the transverse energy. The segmentation of the plot corresponds to θ and ϕ of sections of calorimetry. Remember that each jet has transverse momentum of about 100 GeV, so if our fragmentation estimate is meaningful the half angle of the jet is about 6 degrees. The segmentation in this LEGO plot is 15 degrees in ϕ and 5 degrees in θ. A 200-GeV mass jet should be contained in 1 or 2 of these segments. That's certainly observed to be the case. This plot also indicates how easy it is to observe jets at collider energies. All the debris simply does not appear in this plot. Recall that the mean charged multiplicity for $|y| < 3$ is supposed to be about 30, and yet these soft particles do not appear since they come in at low-transverse momentum and leave no impression on the vertical scale. At SPS energies, 2 jet events just stand out like a sore thumb. This clarity is somewhat in contrast to the situation at Fixed-Target experiments where jets are much harder to dig out.

Matching a detector to jet properties

These considerations lead us to the conceptual design of a general purpose jet detector such as CDF in BØ or the DØ detector. If the luminosity is assumed to be $10^{30}cm^{-2}sec^{-1}$, then a run of 3,000 hours is about 10^7 seconds giving an integrated luminosity of $10^{37}cm^{-2}$. Hence, the maximum detectable cross section is about 10^{-36} cm^2. Using the UA2 data on jets which was shown in Fig. B.5, this means a jet with $\underline{P}_\perp$ of 150 GeV or a jet-jet mass of 300 GeV. A jet of this transverse momentum has a 1/2 opening angle of about 4.7 degrees. That angle corresponds to a slice of rapidity of about 0.08. If we're going to instrument phase space for angles greater than 2 degrees (that means rapidity greater than 4), one has a rapidity span of 8 units. If we take the goal of just containing the 300 GeV jet mass and not learning anything

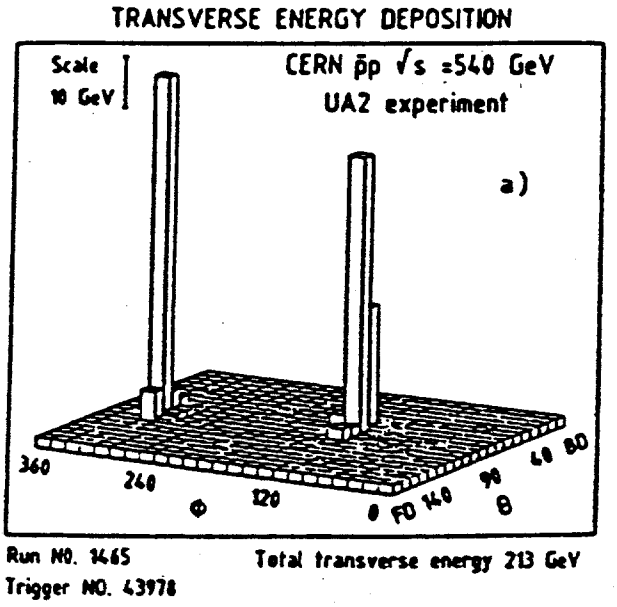

B.11 CERN SPS LEGO plot for total E_T = 213 GeV event.

about its internal substructure then we can calculate the number of "towers" we need. That calculation is sketched out in Eq. B.26.

$$\begin{aligned} M &\sim 300 \text{ GeV} \\ P_\perp &\sim 150 \text{ GeV} \\ \delta_{1/2} &\sim 5^\circ \\ y_{1/2} &\sim 0.08 \\ \theta &> 2^\circ,\ \Delta y = 8 \end{aligned} \qquad \text{B.26}$$

$$[(\Delta y = 8)/(2y_{1/2} = 0.16)] \left[\left(\frac{\Delta\phi}{2\pi}\right)^{-1} = \frac{4^\circ}{360^\circ}\right] = 4500$$

The steps of 0.16 of rapidity cover the total rapidity span of 8. The steps of ϕ are 4 degrees out of 360. Thus, you need 4,500 towers in your "LEGO plot" to resolve such jets. In addition, there needs to be longitudinal segmentation in these towers for purposes of minor experimental details such as separating electrons from hadrons. That increases the number of individual readout segments. Finally if you wanted to resolve particles within the jet, the jet multiplicity would be of the order of 4 or 5. You would have to segment in angles to about 1 degree, which would mean 25 times more towers. It's now reasonably clear why these general purpose detectors have large numbers of towers; they are designed around a study of the jet physics which is accessible with typical $\bar{p}p$ luminosities. As an aside, SSC detectors to handle 1000 times more luminosity and 20 times higher $\sqrt{s}$ (hence $P_\perp$) will have substantially more towers than TeV-I collider detectors like BØ and DØ.

For example, CDF has electromagnetic calorimetry, muon detection toroids, and quark and gluon jet detection using hadronic calorimetry. It also aims to find neutrinos by the fact that there are events with missing transverse momentum. Basically CDF is a detector for standard model particles; quarks, leptons, and gauge bosons. It has a segmentation in rapidity of 0.1 units and an azimuthal segmentation

of 5 degrees and 15 degrees. The segmentation of the various regions of calorimetry is shown in Fig. B.12. What is plotted are the tower sizes in ϕ and θ (ϕ and pseudo-rapidity) for the central, end wall, end plug, and forward calorimeters in CDF. The tower segmentation is almost that which we would expect from the very simple minded hand calculations of containment of the maximum mass observable jet.

The DØ detector is very similar in the segmentation of the towers. It has somewhat finer longitudinal segmentation. It also possesses additional detectors for leptons; transition radiators for electrons and thicker toroids for muons. The idea there is not to segment better but to do finer particle identification. It also has a micro-vertex detector to look for weak decays. In DØ, experimenters will try to take the calorimetry which is detecting quark and gluon jets and use tracking to do flavor tagging of the quarks. They will try to look for heavy flavors using their sequential decays. There has also been an emphasis in the DØ detector on not having any holes, where the particles could sneak out. The attempt is to reduce the missing transverse-momentum signal due to systematic errors below the physics signal due to neutrinos which come from known standard model processes such as heavy-flavor decays. More on this topic will appear in Section C.

The object of the exercise performed in Section B has been to calculate from first principles and from some very simple phenomenology the TeV-I production of heavy flavors and jets. Subsequently, we tried to carry through the jet-decay (fragmentation) estimates. This study will allow us (on the back of an envelope) to calculate the required segmentation for a large general purpose detector. It's gratifying to see that all of these calculations come out to within an order of magnitude. The results of this exercise can easily be extended to the conditions which will obtain at the SSC.

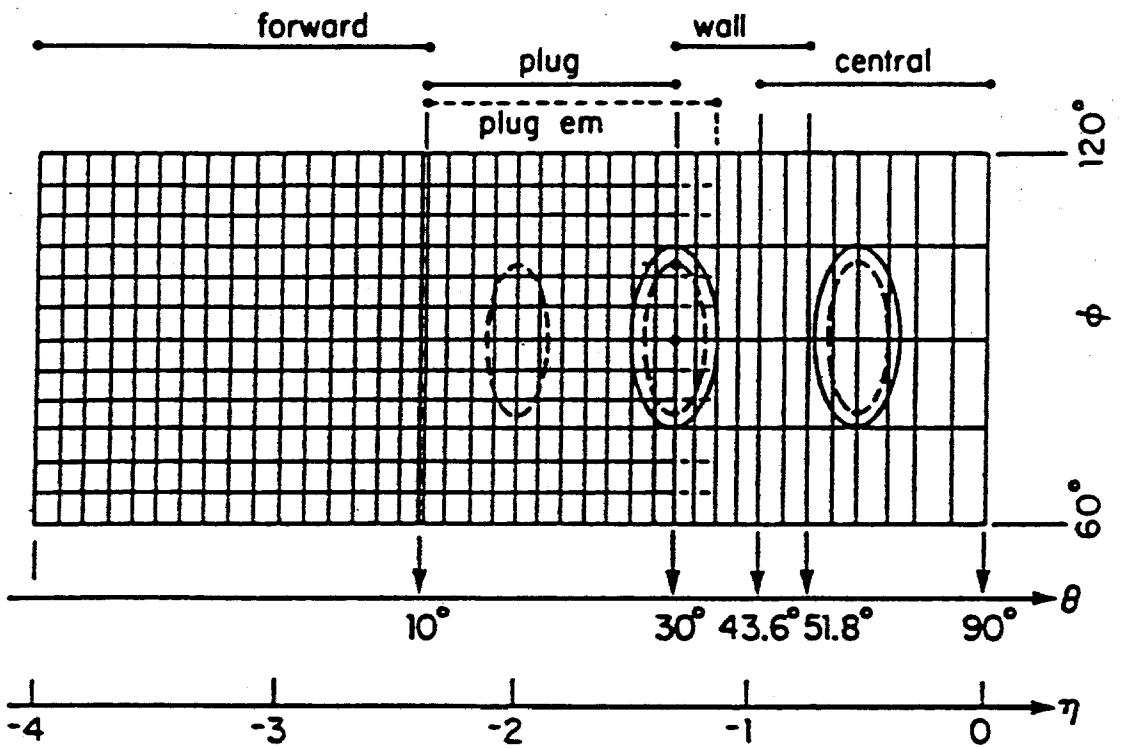

B.12 Calorimeter tower layout for E-741 (BØ).

C. Electro-Weak gauge bosons.

Electro-Weak unification

The electromagnetic interaction with which we are all familiar has a $1/r$ potential. The Fourier transform of that in momentum transfer space is $1/q^2$ which is what we expect for a propagator with zero mass. The weak interaction in contrast was initially formulated as a 4 fermion contact interaction with a δ function dependence of the potential in space. It is perhaps obvious that there is difficulty with divergences in this kind of theory. The most obvious thing to do is to spread out the interaction spatially. One way to accomplish this is to invent a bosonic particle propagator so that the potential goes as $(e^{-r/\lambda\!\!\!^{-}_c})/r$ where $\lambda\!\!\!^{-}_c$ is the Compton wavelength. This is the standard form for a Yukawa potential. In momentum transfer space such a potential goes as $1/(q^2+M^2)$. In the case of the weak interactions, if the force propagator has a mass of 100 GeV, then the Compton wavelength is 0.002 Fermis. The weak interaction is still a very short range potential. At low values of the momentum transfer (on a scale set by the weak boson mass) the electromagnetic and weak potential look radically different. However, if the momentum transfer is much larger than any mass scale, which means if we're at much shorter distances than the Compton wavelength of the W boson, then the electromagnetic and weak potential both have a $1/r$ or $1/q^2$ dependence. This fact holds out the possibility of unifying the weak and electromagnetic interactions. In Eq. C.1 the hypothesis is made explicit.

$$g_W^{\,2} = G_F M_W^{\,2} \qquad \text{C.1}$$

$$\sim \alpha$$

Firstly, the coupling constant g_W is related to the Fermi coupling constant G_F by equating the four fermion point interaction with the form you get with a W propagator. Then the hypothesis that electromagnetic and weak interactions are unified is that this weak coupling constant is of the same order as the electromagnetic coupling constant $\sqrt{\alpha}$. Specifically the electroweak hypothesis is given in Eq. C.2 which relates α to the Fermi coupling constant.

$$\alpha/M_W^{\ 2} = (G_F\sqrt{2}\,\sin^2\theta_W)/\pi \qquad \text{C.2}$$

$$e/\sin\theta_W \sim g_W$$

In this equation, θ_W is the Weinberg mixing angle. Basically, the hypothesis is that there are 4 gauge bosons in SU(2)xU(1). There are then 2 group coupling constants g_W and g_W'. Spontaneous symmetry breaking gives the $W^{\pm}$ and Z^o mass, while γ remains massless. This means that g_W and g_W' are mixed (rotated) such that $e \sim g_W \sin\theta_W$. The angle θ_W is not specified in the standard model. It must be measured. There are many excellent discussions of electroweak physics and we will not say anything more except that $\sin^2\theta_W$ has a value of order 1/5. In grand unified models θ_W is specified. For example in SU(5), $\sin^2\theta_W = 3/8$ at the scale of the unification mass. Renormalization of the weak interactions requires that there are charged W bosons <u>and</u> neutral currents. This means that we need a neutral weak boson called the Z^o. Since $G_F \sim 1\times10^{-5}$ GeV^{-2}, $1/\sqrt{G_F} = 316$ GeV is the weak mass scale. Using $M_W \sim g_W/\sqrt{G_F}$, $M_W = \sqrt{\pi}(g_W/\sqrt{G_F})/2^{1/4} = \sqrt{\pi}(e/\sqrt{G_F}\sin\theta_W)/2^{1/4}$ we find $M_W = 89$ GeV. As seen in Eq. C.3, the typical distance scale for these bosons is about 500 times smaller than that characterizing the size of the proton.

$$\lambda\!\!\!^{-}_W = h/M_W\, c = 0.002 \text{ Fermi} \qquad \text{C.3}$$

W,Z coupling to quarks and leptons

The W and Z gauge bosons then couple to quarks and leptons with coupling constants of order e. In particular they couple universally, independent of color (color-blind). In regard to flavor, the gauge bosons couple to quarks and leptons in a universal manner for allowed couplings. We will simply ignore all disfavored couplings such as $W^+ \to u\bar{s}$ which is responsible for $K^+ \to \pi^+\pi^0$ decay. What is listed in Eq. C.4 is then an enumeration of the allowed coupling of W's and Z's to both quarks and leptons. In this list we have assumed that there are no Cabibbo suppressed possibilities.

$$\begin{array}{lll} W^+ \to u\bar{d}, & Z^0 \to u\bar{u} & d\bar{d} \\ \quad c\bar{s} & \quad c\bar{c} & s\bar{s} \\ \quad t\bar{b} & \quad t\bar{t} & b\bar{b} \\ \quad e\bar{\nu}_e & \quad e\bar{e} & \nu_e\bar{\nu}_e \\ \quad \mu\bar{\nu}_\mu & \quad \mu\bar{\mu} & \nu_\mu\bar{\nu}_\mu \\ \quad \tau\bar{\nu}_\tau & \quad \tau\bar{\tau} & \nu_\tau\bar{\nu}_\tau \end{array} \left.\vphantom{\begin{array}{l}a\\a\\a\end{array}}\right\} \times 3 \qquad \text{C.4}$$

For example, assuming that we multiply the quarks by three for color degrees of freedom, we expect that the purely muonic branching fraction for W's is about 1/12 and the purely muonic branching fraction for Z's is about 1/24.

For the width of the gauge bosons (on purely dimensional grounds) the only mass scale relevant for light decay products, barring dynamics, is the mass of the W itself. We expect that the width will be proportional to the mass. Drawing a diagram for the decay we also expect it to be proportional to the coupling constant squared. In Eq. C.5, the approximate expectation and the exact calculation for the partial decay width of $W \to e\nu$ are given. Note the characteristic $\Gamma \sim g_W^2$ with $g_W \sim e/\sin\theta_W$ behavior.

$$\Gamma(W \to e\nu) \sim g_W^{\,2} M_W \qquad \text{C.5}$$

$$= \alpha M_W/12 \sin^2\theta_W$$

Using M_W = 89 GeV, $\sin^2\theta_W$ = 1/5 and $\Gamma(W \to e\nu)/\Gamma(W)$ = 1/12, we estimate $\Gamma(W) \sim 3.2$ GeV. These expectations for the mass and width of both $W^{\pm}$ and Z^{o} have been spectacularly confirmed at the CERN collider.

Production of W and Z at the Collider

Looking at the possible couplings listed in Eq. C.4 it is easy to see that copious production of W's will occur (by valence quarks) in proton antiproton collisions only with the $u\bar{d}$ and $d\bar{u}$ combinations. A rough estimate is very similar to that already made for heavy flavor quark pairs (see Eq. B.19) with the replacement of the strong coupling constant by $g_W^{\,2}$. That estimator is given in Eq. C.6, assuming M_W = 100 GeV.

$$\sigma(W) \sim g_W^{\,2}\left[\frac{\tau}{M^2}\,\frac{dL}{d\tau}\right]_{u\bar{d}+d\bar{u}}$$

$$\left(\frac{\tau}{M^2}\,\frac{dL}{d\tau}\right)_{u\bar{d}} \sim 2 \times 10^7 \text{ nb}/[M\ (\text{GeV})]^{2.8} \qquad \text{C.6}$$

$$g_W \sim e/\sin\theta_W$$

$$\sigma(W) \sim 3.7 \times 10^{-33}\ \text{cm}^2$$

The scale for the production of weak bosons at TeV I is then 10 nb. The precise calcuation is quoted in Eq. C.7 which is taken from the paper of EHLQ.

$$\sigma(W) = \alpha\left[\frac{\pi^2}{3\sin^2\theta_W}\right]\left(\frac{\tau}{M_W^2}\frac{dL}{d\tau}\right)_{u\bar{d}+d\bar{u}}$$

$$\sigma(W) = 6.3 \times 10^{-33}\ cm^2\left[\tau\frac{dL}{d\tau}\right]_{u\bar{d}+d\bar{u}} \qquad C.7$$

A simple hand calculation estimate for the production of W bosons comes from a minor modification to Eq. B.13 which had to do with the strong interaction production of vector mesons. The formula which is obtained using Eqs. B.13, and C.5 is given in Eq. C.8.

$$xu(x) = a\sqrt{x}(1-x)^3$$

$$xd(x) = b\sqrt{x}(1-x)^4 \qquad C.8$$

$$\left(\frac{d\sigma}{dy}\right)_{y=0} = \frac{8\pi^2 ab(e/\sin\theta_W)^2(1-\sqrt{\tau})^7\sqrt{\tau}}{3M^2}$$

Compared to "radiated" sources like gluons (see Eq. B.13) there is a $\sqrt{\tau}$ factor in Eq. C.8. If τ is large, then valence sources dominate production ($\langle x\rangle \sim \sqrt{\tau}$). If the particles are "light" w.r.t. $\sqrt{s}$, then $\langle x\rangle$ is small, and "sea" sources dominate. We parameterize the valence u quark distribution as a power law and the d quark distribution as a steeper power law. This takes into account the observation at SLAC that u quarks dominate as x approaches one. To get the total width to put into Eq. B.13, we have taken the partial width of Eq. C.5 and the counting fraction branching ratio from Eq. C.4 to yield the production cross section of W's, ($d\sigma/dy$) at y=0. In Fig. C.1 is shown the exact prediction for the production cross section for W and Z gauge bosons in $\bar{p}p$ interactions as a function of $\sqrt{\tau}$. Over most of the range of this figure, we are in the sea dominated regime (see Fig. B.1). We approximate this fact by removing the factor of $\sqrt{\tau}$ from Eq. C.8 (see Eq. B.13). Also shown in

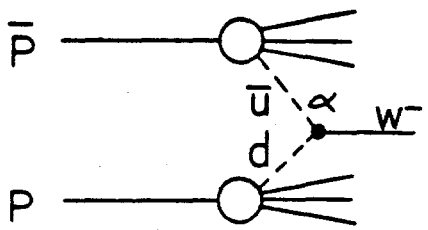

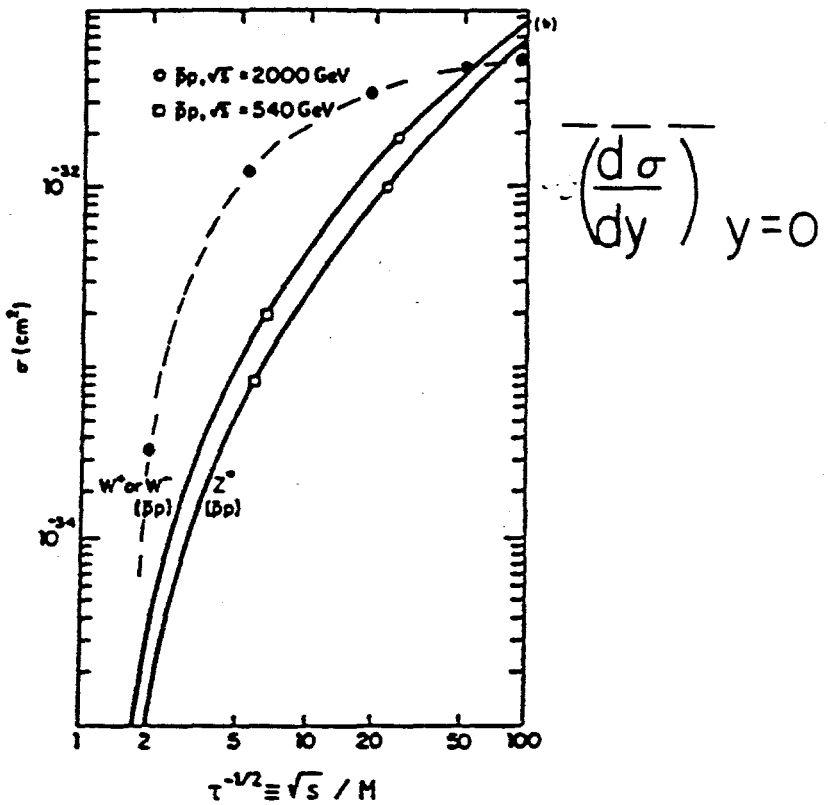

C.1 Production cross sections for electroweak gauge bosons as a function of $(\sqrt{\tau})^{-1}$.

Fig. C.1 is this modified functional dependence. One can see that this estimate meets our ground rules of being within an order of magnitude of the exact calculation. However, in contrast to gluon fusion, the energy dependence is due to a complex mix of sea and valence sources. One obvious thing to note is that the TeV-I collider has an order-of-magnitude advantage over the CERN SPS collider in the raw production cross section for electroweak bosons. As with heavy flavors, a study of Fig. C.1 will convince you that this big advantage disappears far above threshold; at the SSC W's will be "light" particles with only weak energy dependence.

W backgrounds

What are the backgrounds to observing W bosons? Since the neutrinos can't be directly observed and the leptons will be seen at high $p_\perp$ via the Jacobean peak (i.e., $P_\perp \sim M/2$ peaking), the background will be anything that produces single leptons at high $p_\perp$. For example, jets can make high $p_\perp$ leptons via heavy flavor decays. The jet production cross section has already been discussed. There is a sequence of decays which has to occur to make a high $p_\perp$ lepton. First the outgoing gluons from the jets have to fragment into a leading heavy quark. Assuming they are flavor blind this happens about 1/5 of the time as defined in Eq. C.9. After the gluon fragments into a leading b quark, the b quark has to semileptonically decay. A similar color counting as used in Eq. C.4 leads one to estimate the branching ratio for this decay to be about 1/9 (which is certainly consistent with the data from the e^+e^- colliders).

$$B(g \to b) \sim (1/5) \qquad \text{C.9}$$

$$B(b \to cW \to c\mu\nu) \sim (1/9)$$

What is happening is illustrated graphically in Fig. C.2. Gluon jets fragment into leading charged particles, in this case b quarks. They fragment with some probability. The b then semileptonically decays into leptons with a second branching ratio. The fragmentation goes from 60-GeV $p_\perp$ to say 30-GeV $p_\perp$ for the leading b fragment. Then the b with 30-GeV $p_\perp$ suffers a three-body decay degrading it to a 10-GeV $p_\perp$ electron. The smooth curves are the result of a detailed Monte Carlo and it's gratifying that we're in the ball park with these crude estimates. Note that at a given $P_\perp$ this decay sequence means jets are ~ 100 times more copious than single particles, and e are 1000 times rarer again.

W signal from inclusive leptons

The electroweak production cross section has already been estimated at 10 nanobarns. The branching ratio into $e\nu$ is estimated from color counting to be 1/12, so that the cross section times branching ratio is 0.8 nanobarns. The Jacobean peak should occur at a $p_\perp$ roughly half the mass of the W boson, which in this case is degraded slightly to about 35 GeV. W production is spread over a range of rapidity of about 4. If one takes the smear of the Jacobean peak due to decay kinematics and production $p_\perp$ from the initial system (see Figure C.5 and a later discussion) then an estimate of the W signal is $d\sigma/dydP \sim 0.8$ nanobarn/$(\Delta y = 4)(\Delta P_\perp = 10)$. This estimate for the W differential cross section of 2×10^{-35} cm^2 is shown in Fig. C.2. It's reasonably clear that the W decay should stand out above the known backgrounds. In Fig. C.3, data from UA1 on jets (which we've already seen), and single high $P_\perp$ muons is shown with the same sort of sequential decays indicated as in Figure C.2. The estimate is useful but it's not quite as accurate as in Fig. C.2. Data are always more useful than a Monte Carlo. However the main features of the relationship between jets and single high $P_\perp$ leptons is confirmed by the UA1 data.

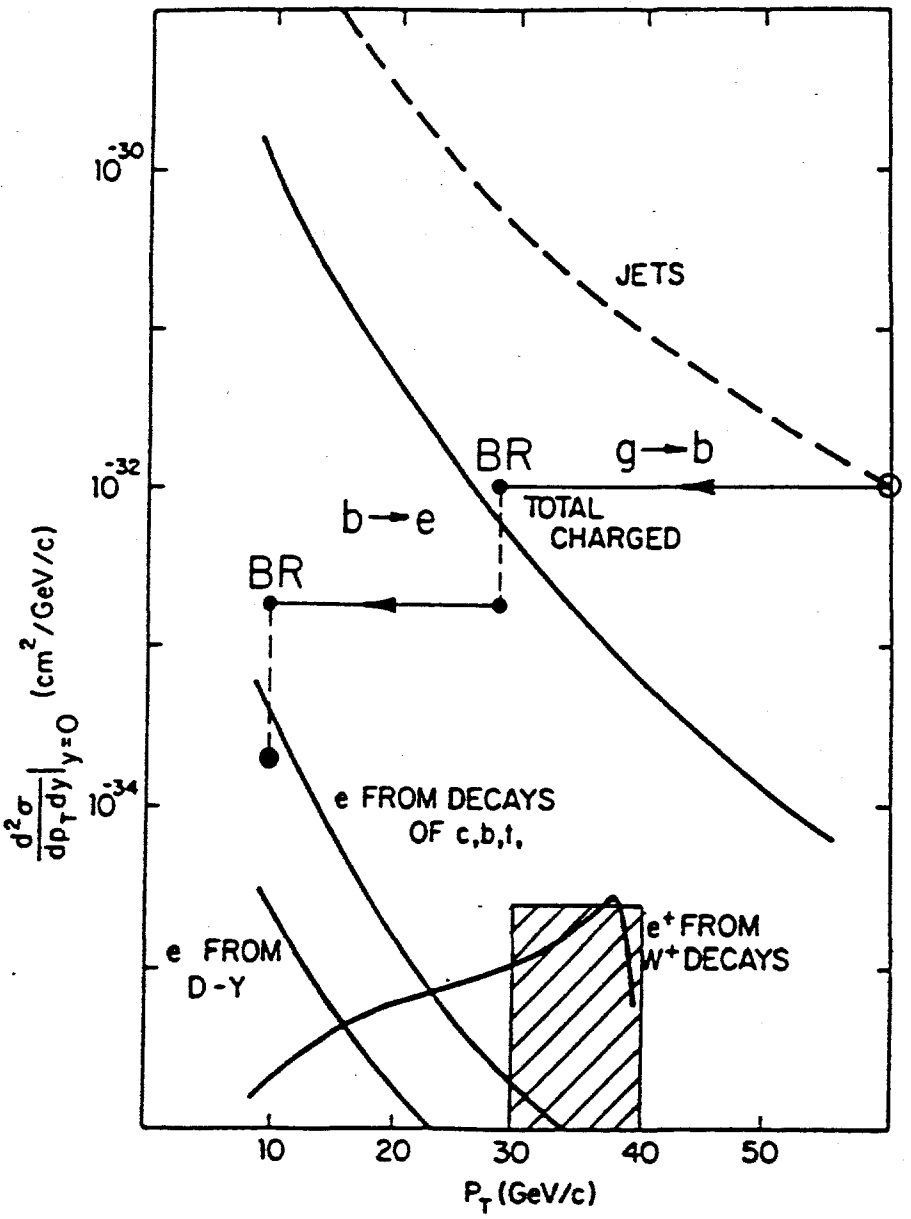

C.2 Production of high $P_\perp$ electrons as a function of $P_\perp$ for jets and $W^\pm$ bosons.

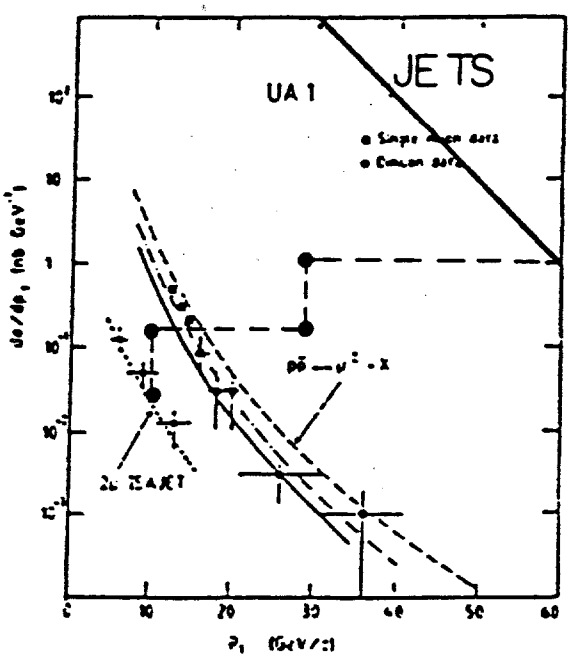

C.3 UA1 data on cross section for jets and $\mu^{\pm}$ as a function of $P_{\perp}$.

In Fig. C.4 data on the missing transverse energy distribution is shown. In these events there is also an isolated electron candidate required with a $p_\perp$ greater than 15 GeV. So what's really plotted here is the transverse momentum distribution of the neutrino. We see a nice Jacobean peak, as one expects from two-body kinematics if there is very little transverse momentum of the parent. However, we should note that there is another possible decay, which lepton universality says should happen with equal branching fraction. The decay is $W \to \tau\nu$ where the τ subsequently decays with a 20% branching ratio into electron and neutrinos. The decay chains are indicated in Eq. C.10.

$$
\begin{array}{l}
W \to \tau\ \nu \to (e\bar{\nu})\nu \\
\tau \to W^-\nu \\
\quad\ \ \hookrightarrow (\bar{u}d)\ \mathrm{x}3 \\
\qquad\quad e\nu \\
\qquad\quad \mu\nu
\end{array}
\qquad \text{C.10}
$$

That means that this nice peak will be smeared out somewhat because you will have a three body final state due to the sequential τ decay at the 20% level.

An indication that the hard-scattering production mechanism is as assumed is shown in Fig. C.5. This Figure is also after the fact justification for looking for a Jacobean peak. What is shown is UA1 data for the transverse momentum of the W boson parent. On the scale of the W mass the transverse momentum is quite small. We have already explicitly ignored "intrinsic" parton transverse momentum. The W can be given a transverse momentum by gluon radiation in the initial state. The curve of Figure C.5 is a Monte Carlo result which incorporates such effects.

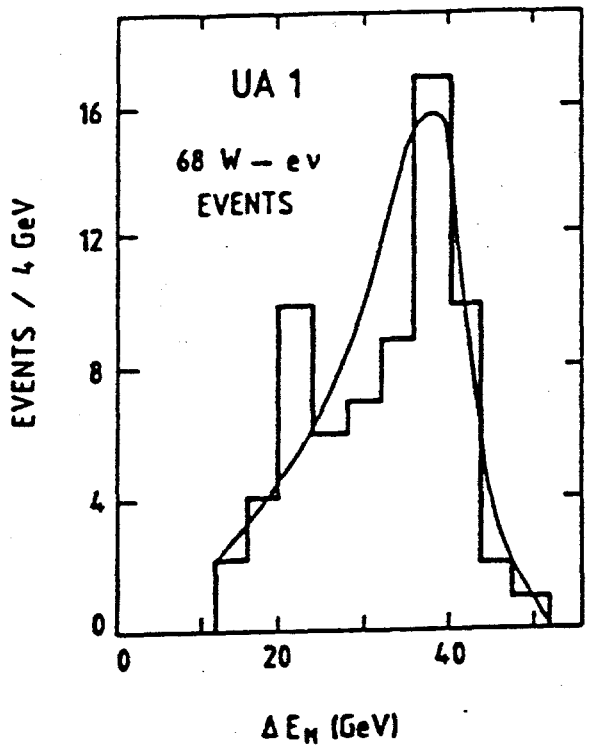

C.4 UA1 data on missing E_T (ν.$P_\perp$).

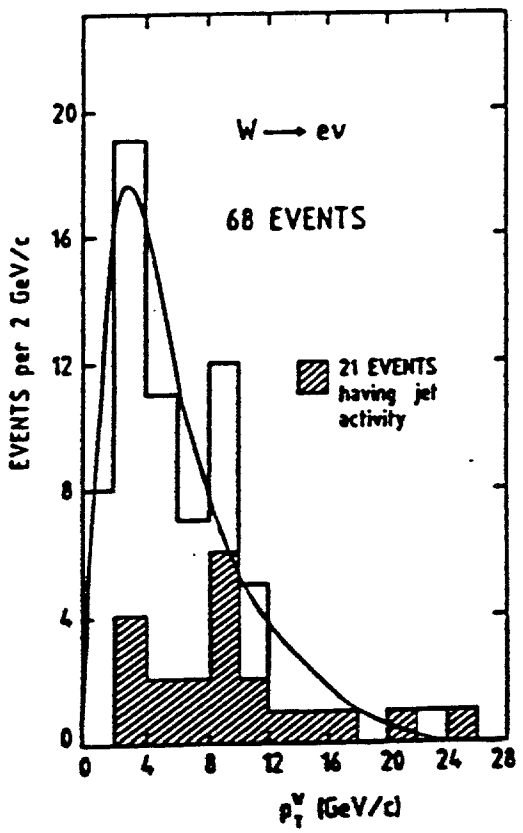

C.5 UA1 data on $P_\perp$ of $W^\pm$.

x distribution for W production

What prediction can we make for the x distribution of the W boson? If we refer back to Eq. B.11, we can immediately write down Eq. C.11 for $d\sigma/dx$ of the W bosons. Assuming that the u quarks and d quarks have the valence like power laws shown in Eq. C.8, we can predict the shape of the x distribution for the W bosons.

$$\frac{d\sigma}{dx} \sim \left[\frac{x_1 F(x_1) x_2 F(x_2)}{x_1 + x_2}\right] \sim \frac{(1-x_1)^{n_1}(1-x_2)^{n_2}}{\sqrt{(x/2)^2 + \tau}} \qquad \text{C.11}$$

That shape is shown in Fig. C.6 along with data and more detailed theoretical calculations. It's extremely nice to see that we can simply understand the observed shape. Note that for values of x which are large with respect to τ, x_1 from the incoming particle number one approaches x, while x_2 approaches τ/x which is small and can be approximated as zero. In that approximation $d\sigma/dx$ has an x dependence as seen in Eq. C.12. Note that at Tev I, τ for the W is ~ 0.002.

$$x_1 \to x, \; x_2 \to \tau/x \sim 0$$

$$\left(\frac{d\sigma}{dx}\right)_{x \gg \tau} \sim \left[\frac{(1-x)^3 + (1-x)^4}{x}\right] \qquad \text{C.12}$$

Recall that for x=0, $x_1 = x_2 = \sqrt{\tau} = M/\sqrt{s}$. Hence at x=0 (at the Collider) the sea quarks dominate. However for production at finite x, $x_1 \sim x$ and valence sources rapidly become important.

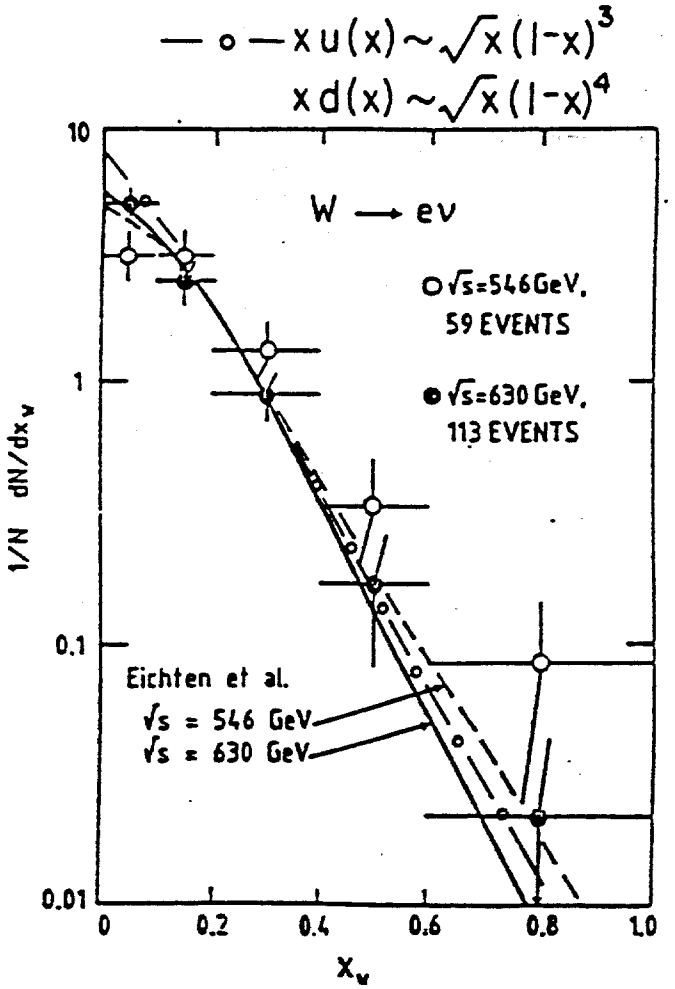

C.6 Data on the x distribution of $W^{\pm}$ from the SPS Collider experiments.

W→eν angular distribution

The UA1 data on the angular distribution of leptonic W decays is further evidence that these are indeed W bosons and that the leptons have a well defined helicity which is forced upon them by the V-A nature of the weak interaction. The V-A structure of the charged weak current means that all fermions are left-handed (they have a helicity of minus 1/2) and all anti-fermions are right-handed (they have a helicity of plus 1/2). As we can see, looking at Fig. C.7, in $\bar{p}p$ collisions, assuming valence sources, the positron, in order to conserve angular momentum, will need to come out along the $\bar{p}$ direction whereas the electron will need to come out along the proton direction. The decay angular distribution will go like $(1 \pm \cos\theta)^2$. The data from UA1 follow this expectation very nicely. The formula for the differential decay rate is given in Eq. C.13.

$$\frac{d\Gamma}{d\Omega} \sim (1 \pm \cos\theta)^2 \qquad \text{C.13}$$

Note that production from sea quarks will confuse this simple picture and wash out the asymmetry. However requiring x of the W to be > 0.3 will insure valence quark dominance as we have previously discussed. Since glue couples only to color, this source is irrelevant for weak interactions.

$W \to t\bar{b}$

The reason we have not made any discussion of other decay modes of the W is simply that they have yet to be seen. The W cross section is of order 10 nanobarns. Using the flavor blind property of the decays, the lowest background large branching fraction decay would be $W \to t\bar{b}$, which should have a branching fraction of about 25%. If we can reliably tag heavy-flavor decays by using a vertex detector, then the background should be reduced. Assuming a 10-GeV mass resolution on the $t\bar{b}$ final

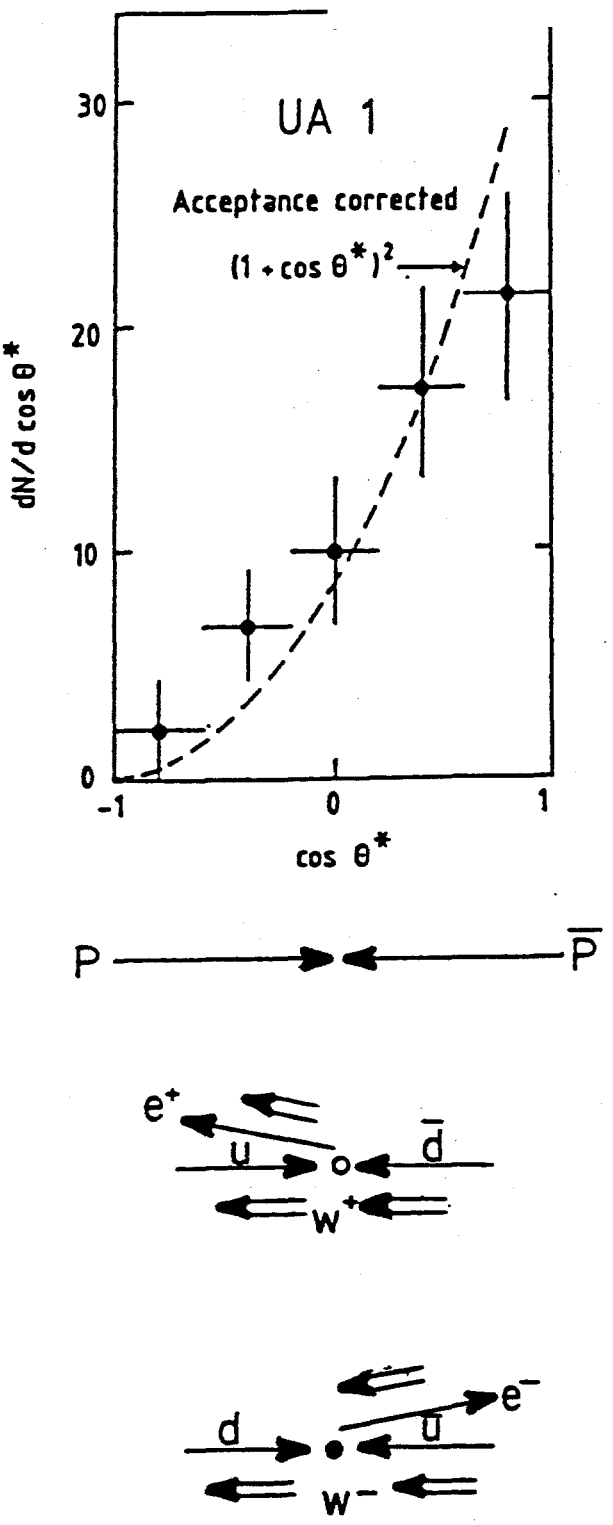

C.7 Data on the decay angular distribution for $W^{\pm}\to e^{\pm}\nu$ decays.

states, the cross section times branching ratio for the W divided by the mass resolution is $B d\sigma/dM \sim 1/4$ nanobarn/GeV. The problem is simply that the jet-jet mass distribution has a cross section which is about two orders of magnitudes higher at twice the mass. These jets (assuming flavor blind gluons) have about 1/5 probability to fragment into t, while the other jet has about 1/5 probability to fragment into $\bar{b}$. The joint probability for $jj \to t\bar{b}$ is down by a factor of 1/25. The mass of the two leading fragments is degraded roughly a factor of two from the jet-jet mass. Unfortunately, even with these suppression factors the W decay is still buried by a factor of at least five.

One needs enormous statistics or some way to reduce the mass resolution. Note that the mass resolution depends on both the detector and on the algorithm that assigns tracks to jets. We have already mentioned that soft fragments of jets can be lost in the debris. Referring to Figure B.6, there are $n(2n - 1)$ pairwise mass terms, $n(n - 1)$ of which sum to two zero jet masses, and n^2 of which give the jet-jet mass. Suppose you lose 1 track. This loss pulls the mass by $\delta M/M \sim 1/2n$. Assuming $n=3$, then the jet-jet mass has a FWHM of $\sim$ 30 GeV at the W mass. Clearly the jet finding strategy is crucial for reduction of δM. As yet no one has succeeded in reconstructing a W signal from jet-jet masses. This is a challenge for the TeV-I physics program.

High- mass dilept

Let us turn now to the study of high-mass dileptons at colliders. The obvious background for this process (from what we have already discussed in the case of single high $p_\perp$ leptons) is again due to jets. It turns out to be miniscule however; the differential cross section, $d\sigma/dM$ where M is the jet mass has already been noted. At 300 GeV at the collider, we expect a cross section of about $5 \times 10^{-37} cm^2/GeV$.

This is the sort of estimate we've already made in Section B. The probability of the gluon fragmenting into a heavy flavor such as b is about 1/5 and again the branching fraction for heavy flavors such as b goes to electron is about 1/9 (see Eq. C.9). The joint probability for both gluon jets to fragment into a heavy quark followed by decay to an electron is about 1/2025. As shown in Eq. C.14, we have a mass spectrum for unlike sign di-electrons of about $3 \times 10^{-40}\,cm^2/GeV$ at a mass reduced from the 300 GeV jet-jet mass down to 50 GeV di-electron mass.

$$\left(\frac{d\sigma}{dM}\right)_{jj}[B(g\to b)]^2[B(b\to ce\nu)]^2 \qquad \text{C.14}$$
$$m_{ee} \sim M_{jj}/6$$

The cross section for jets and for background electrons due to jets using this estimate (dashed line) is given in Fig. C.8 along with detailed Monte Carlo results (solid line). This background is negligible.

What about direct production of high-mass electron-positron pairs? This process goes by the name of Drell-Yan production. The cross section estimate for Drell-Yan production is as indicated in Eq. C.15.

$$\left(\frac{d\sigma}{dM}\right)_{DY} \sim \frac{\hat{\sigma}(\tau dL/d\tau)_{u\bar{u}}}{M} \qquad \text{C.15}$$
$$\sim \frac{4\pi\alpha^2}{3M^3}\left(\tau\,\frac{dL}{d\tau}\right)_{u\bar{u}} \quad (e_i^2 = 4/9)$$

It goes generically as the hard scattering cross section $\hat{\sigma}$ times the differential luminosity divided by the mass. In this particular case the hard scattering cross section is just that for electron positron annihilation, $\hat{\sigma} = (4\pi\alpha^2/3\hat{s})e_i^2$ where e_i is charge of the annihilating quark-antiquark pair. Drell-Yan production has a scaling property that $M^3(d\sigma/dM)$ is a function of τ only. Some data on Drell-Yan production

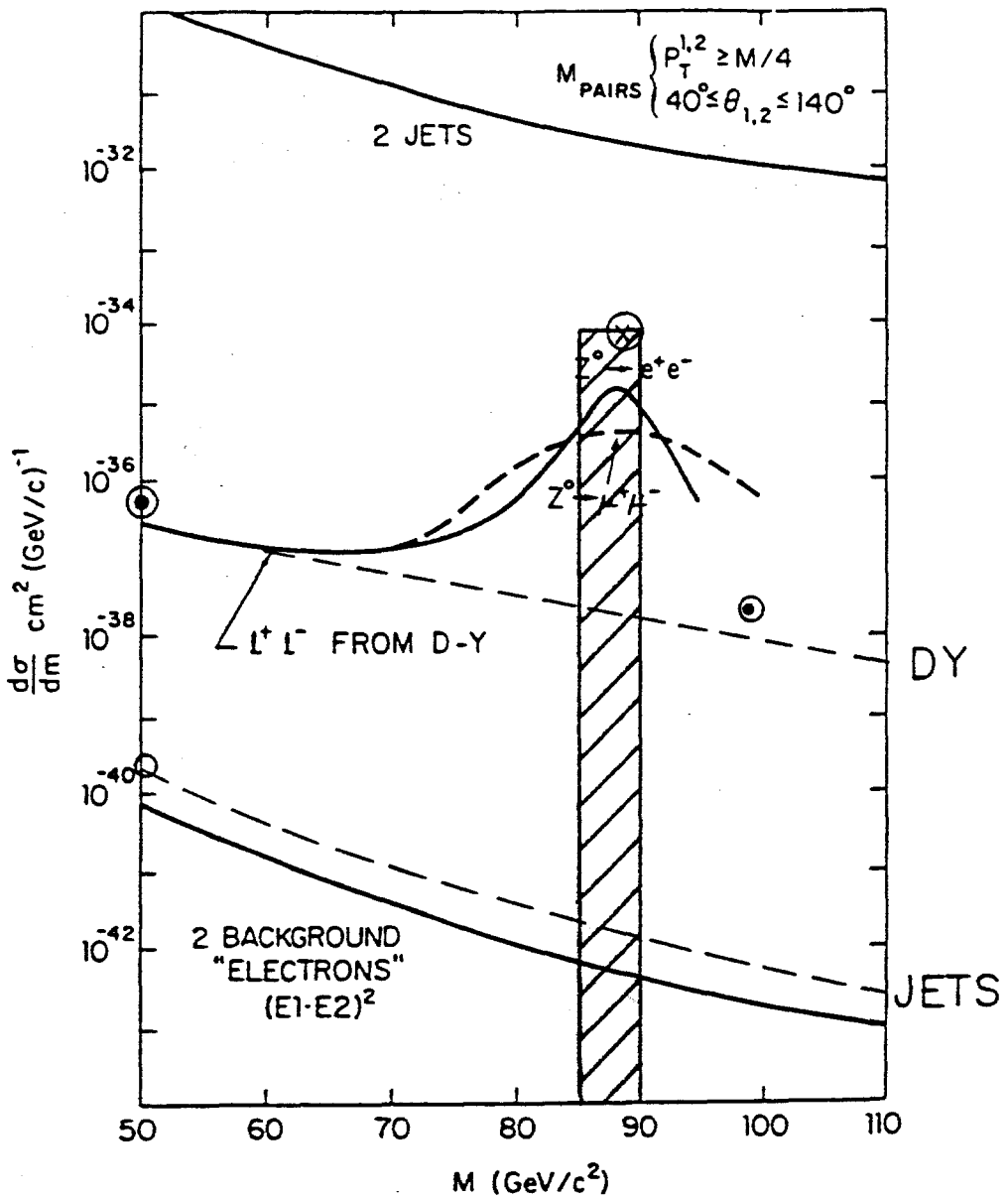

C.8 Production cross section for dilepton pairs due to Z^o, Drell-Yan, and jets.

at Fermilab Fixed-Target energies from E-288 are shown in Fig. C.9. This data plotted as a function of τ has a scaling property which, when integrated over y, is given in Eq. C.16.

$$M^3\left(\frac{d\sigma}{dM}\right)_{DY} = f(\tau) \qquad \text{C.16}$$

The quark-antiquark annihilation cross section (evaluated numerically) is (87 nanobarns/$\hat{s}$)e_i^2 where $\hat{s}$ is given in GeV^2 units. At a mass M = 100 GeV, using the differential luminosity for $u\bar{d}$ from Eq. C.6, the cross section for Drell-Yan production is 4.8×10^{-38} cm^2/GeV. At a mass of 50 GeV we estimate the cross section to be 8×10^{-37} cm^2/GeV. These rates are ~10,000 times larger than the jet backgrounds. They are also shown in Fig. C.8. The estimates are close to the exact calculations.

Z^o signal in lepton pair decays

Finally we estimate the cross section for Z^o production with subsequent decay into electron-positron pairs. We've already estimated the gauge boson production cross section to be at the 10 nanobarn level. Color counting gives us a branching fraction into electron positron pairs of about 1/24 (Eq. C.4). We also made a dimensional argument that the width of the gauge boson would be of order 1 GeV (Eq. C.5). These estimates are shown below.

$$\sigma(Z) \sim \alpha\left(\frac{\tau}{M^2}\frac{dL}{d\tau}\right)_{u\bar{u}}$$

$$B(Z \to ee) \sim 1/24 \qquad \text{C.17}$$

$$\Gamma_Z \sim \alpha M$$

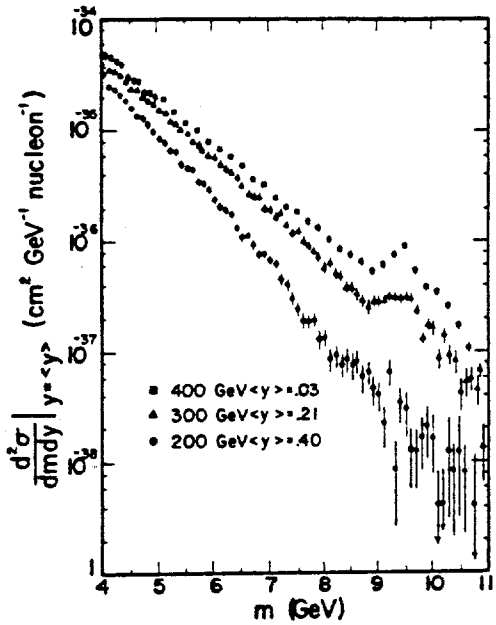

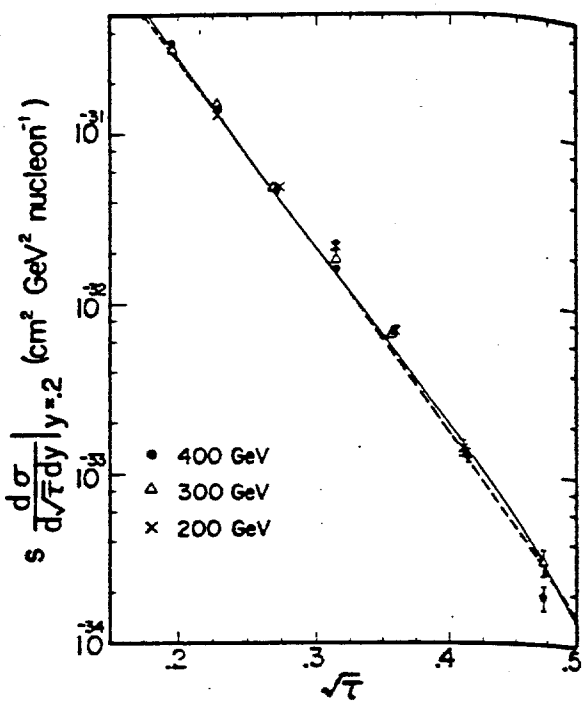

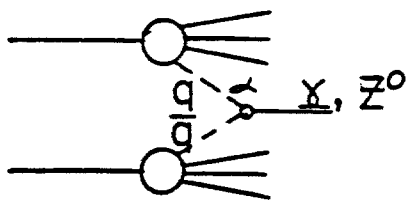

C.9 a) Data on the cross section of dimuons in pp collisions as a function of the mass of the dimuons at various $\sqrt{s}$ values.

b) Scaling property of dimuon production.

Putting that all together we get a cross section times branching ratio divided by natural width of $4 \times 10^{-34} cm^2/GeV$. However, there is an experimental resolution just due to the apparatus which is of order 5 GeV, full width at 1/2 maximum (FWHM), which reduces the signal by spreading it out in mass to be of order $8 \times 10^{-35} cm^2/GeV$ at the peak. These estimates for Z^o production and decay into e^+e^-, Drell-Yan background, and jet background are all shown in Fig. C.8. The first thing one can see is that the hand estimates are in fact rather close to the detailed Monte Carlo results. The second thing to remark on is that the Z^o should stand out well above background; remember that the vertical scale is a log scale. Note that even the dimuon spectrum, with much worse mass resolution, is comfortably above the DY background. UA1 data on Z^o production is shown in Fig. C.10. Indeed there is only a small background. The Z^o appears as a beautiful isolated peak at the appropriate mass. Our expectations about backgrounds are well satisfied. Note that Z^o decays into τ pairs will lead to a final state with e^+e^- pairs and 4 unobserved neutrinos. The e^+e^- pair will have reduced mass which should somewhat fill in the valley between the background and the Z^o peak due to the direct decays into e^+e^- pairs.

Parenthetically, Z^o decay into τ pairs should exist. We've estimated the τ branching ratio into hadron plus neutrino already by color counting to be 60%. That would lead, within the context of the standard model, to missing $p_\perp$ with no lepton tag, which could be confused with an exotic process. However, such a signature does exist at a calculable cross section. The same comment holds true for W decays into $\tau\nu$ where the τ then decays to hadron plus neutrino. This process again leads to missing $p_\perp$, a hadron jet, and no lepton tag. A glance at Eq. C.4 indicates that $Z \to \nu\bar{\nu}$ decays will lead to missing $P_\perp$ with no jets or lepton tags. This all means that the standard model itself is not "hermetic" but leaks out ν without observable μ or e leptons to tag them.

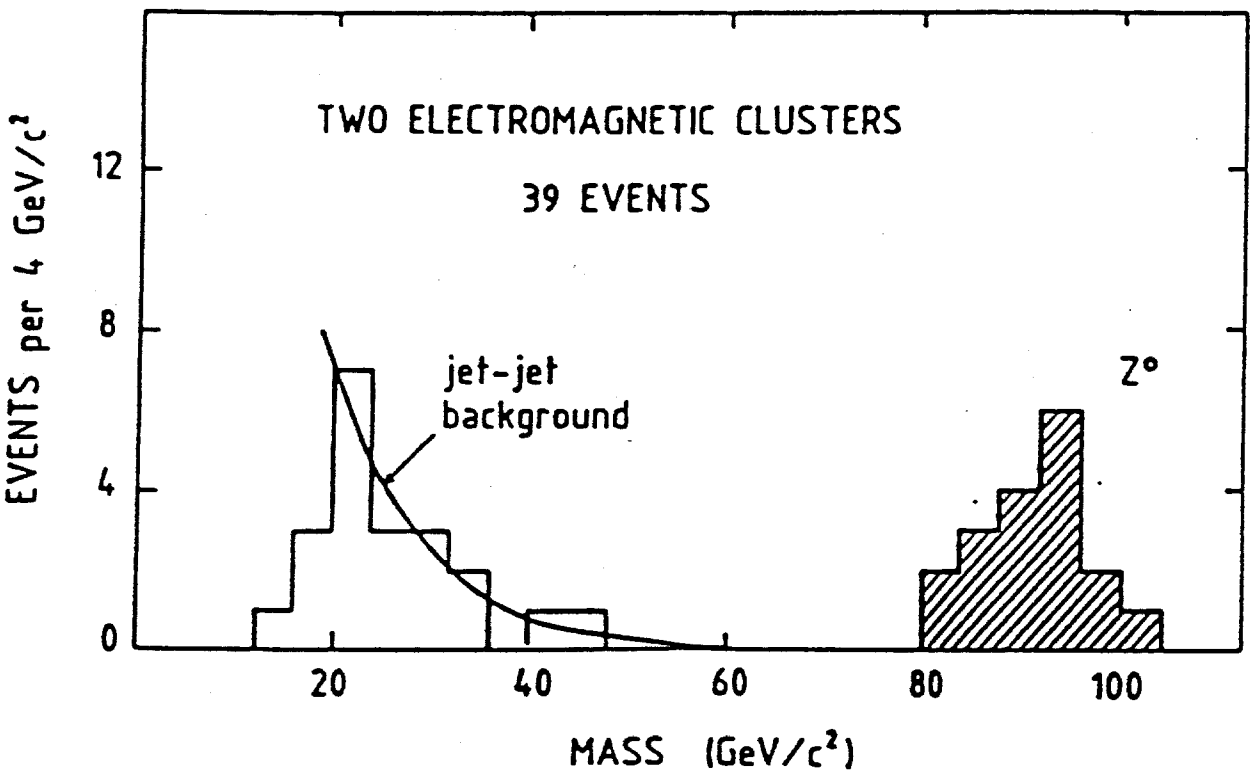

C.10 Data on the cross section for dileptons from the CERN SPS Colliders.

Like-sign dileptons

The organization of the first three generations into weak isotopic doublets is given in Eq. C.18 for the quarks and leptons.

$$(Q/e) = \begin{pmatrix} 2/3 \\ -1/3 \end{pmatrix} = \begin{pmatrix} u \\ d \end{pmatrix} \begin{pmatrix} c \\ s \end{pmatrix} \begin{pmatrix} t \\ b \end{pmatrix} \overset{W\pm}{\updownarrow} \qquad \text{C.18}$$
$$= \begin{pmatrix} 1 \\ 0 \end{pmatrix} = \begin{pmatrix} e \\ \nu \end{pmatrix} \begin{pmatrix} \mu \\ \nu \end{pmatrix} \begin{pmatrix} \tau \\ \nu \end{pmatrix}$$

W's mediate decays as shown from the top row, $Q = (2/3)e$ to the bottom, $Q = (-1/3)e$. Thus, for example, the sequential decay of the t can go top to bottom, bottom to charm, charm to strange as indicated as in Eq. C.19.

$$\begin{aligned} t &\rightarrow bW^+ \\ &\quad\ \hookrightarrow cW^- \\ &\qquad\quad \hookrightarrow sW^+ \end{aligned} \qquad \text{C.19}$$

Thinking about this decay chain, heavy flavor can lead to multileptons in the final state. So far we've only talked about unlike-sign dileptons, but in fact there are more complicated signatures which exist within the context of the standard model.

For production of $c\bar{c}$ pairs the only possibility (looking at Eq. C.19) is the production of unlike-sign dileptons. However $b\bar{b}$ pairs can produce final states with up to four leptons, two of each charge, and for $t\bar{t}$ pairs up to six leptons, three of each charge. Thus within the confines of the standard model there is a well defined mechanism for the production of like-sign dileptons from $b\bar{b}$ and $t\bar{t}$ pairs. The only question is whether the observation of like-sign dileptons is on the scale expected for this process. From the estimates we've made for backgrounds to Z^o from jets (see Eq. C.14) we could just as easily have had a subsequent semi-leptonic decay with a fluctuation to hard fragmentation. This kind of reasoning leads you to believe that the spectrum for like-sign dileptons should not be dramatically different in shape or cross section value (at the large dilepton masses accessible to $b\bar{b}$ and $t\bar{t}$) from the

unlike-sign background due to di-jets which we have already estimated for Drell-Yan background. This expectation is validated by a detailed Monte Carlo evaluation of the like-sign and unlike-sign mass spectrum of dimuons. At UA1, both like and unlike-sign dimuons have been seen. The question is a quantitative one. Can the like-sign dimuon signal be explained within the context of the standard model by known processes? This is a detailed question which can only be answered by a quantitative confrontation of the data with the models.

Trilinear boson coupling

What in addition can we learn about the coupling of electroweak gauge bosons, one to the other? The unification of weak and electromagnetic interactions implies that we will have trilinear gauge boson couplings. These trilinear couplings will manifest themselves as gauge boson pair production. The parton model diagrams for pair production of W's or W's and Z's, or W's and γ's are shown in Fig. C.11. A cross section estimate for these processes is given in Eq. C.20.

$$\begin{aligned} \sigma(WW) &\sim \alpha^2 \left(\frac{\tau}{M^2} \frac{dL}{d\tau} \right)_{M \sim 2 M_W} \\ &\sim \alpha \frac{\sigma(W)}{(2)^{3.5}} \end{aligned} \qquad \text{C.20}$$

It's easy to see that in comparison to production of single gauge bosons this process is down by a factor of α and a factor due to the increased mass of the system. Also shown in Fig. C.11 are the predicted cross sections as a function of the center-of-mass energy for Wγ, WW, WZ, and ZZ pair production. As a rough estimate we have taken Wγ pair production to be just $\sigma(W)$ times α since the Wγ mass can be very small. The W pair production cross section has α times a flux factor due to the fact that one is producing twice as heavy a mass. These factors reduce the cross section with

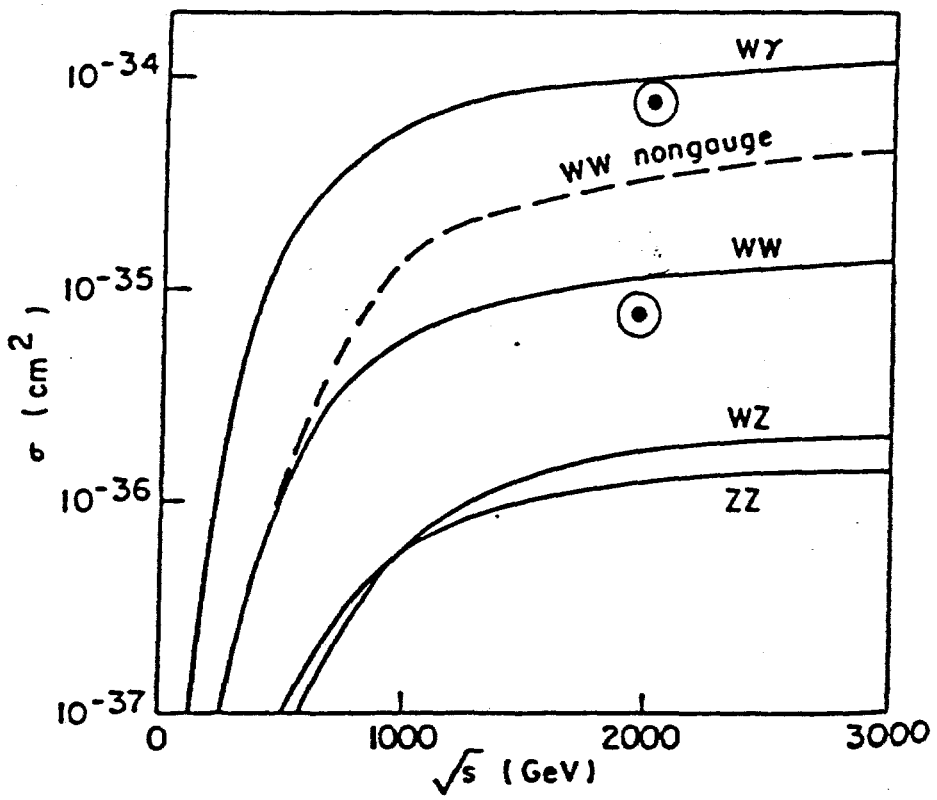

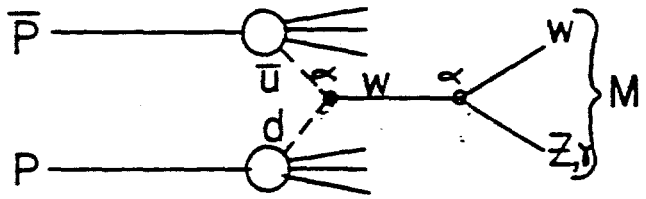

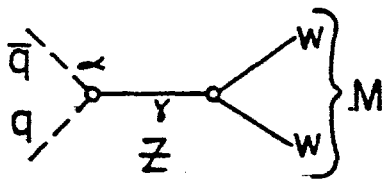

Predicted cross section for gauge boson pairs as a function of $\sqrt{s}$.

respect to single W production by a factor of 1550. These crude estimates appear to come out within a factor of two of the real detailed calculations of the cross section for electroweak boson pair production.

Note that in this case, in particular, the Fermilab Collider is much better off than the CERN SPS Collider. There is an enormous rate premium to be paid for the increased center-of-mass energy when one is dealing with gauge-boson pairs due to the sharp threshold behavior. The detection of WY pairs seems to be well within the luminosity reach of the Tev-I collider and depends only on the existence of excellent photon detection at low momenta so that the WY mass can be allowed to be essentially equal to the W mass. There's some interesting dynamics in the WY system in that there is a minimum in the angular distribution at $\hat{t}/\hat{u} = 2$. Here $\hat{t}$ refers to the momentum transfer between the incident u and the outgoing W. The detection of this process, $u\bar{d} \to W^+\gamma$, will make interesting fundamental tests of the trilinear bosonic coupling (WWY) and of the prediction for the angular distribution. For an integrated luminosity of $10^{37}cm^{-2}$, one will have ~ 100 W^+W^- pairs. If only e and μ can be used to find the W, then only $3(W^+ \to l^+\nu)$ $(W^- \to l^-\nu)$ will be seen. Clearly being able to dig out decays with 1/4 branching ratio $(W \to t\bar{b})$ would be a boon.

Higgs particles

What about the Higgs scalar? This is after all the fundamental scalar which is responsible for the spontaneous symmetry breaking and whose vacuum expectation value gives masses to the gauge bosons. The Higgs boson is supposed to couple to the W's, Z's, quarks and leptons. Unfortunately, the Higgs mass is a free parameter in the standard model and no one has an idea what it is. The scale is probably set by the vacuum expectation value of the Higgs field or by $1/\sqrt{G_F} = 316$ GeV, so we expect the Higgs mass (in the absence of any other knowledge) to be of this size. The width of

the Higgs, by dimensional arguments which we've made before, should be $\sim \alpha M_H$. We've always made these arguments in the absence of any dynamics. Unfortunately for us, the dynamics specified by the standard model says that there is an additional factor of lepton mass m_ℓ over the W mass squared. The dynamics forces the Higgs to preferentially couple to the heaviest available lepton. This means that, if the Higgs mass is less than twice the W mass, the Higgs is favored to decay into the heaviest quark, or $t\bar{t}$ pairs. The width is given in Eq. C.21a.

$$\Gamma(H^0 \to \ell\bar{\ell}) \sim \alpha \left(\frac{M_\ell}{M_W}\right)^2 M_H \qquad \text{C.21a}$$

$$\Gamma(H^0 \to W^+W^-) \sim \alpha \left(\frac{M_H}{M_W}\right)^2 M_H \qquad \text{C.21b}$$

If the Higgs is heavier than twice the W mass, then the favored decay is into weak-gauge boson pairs. The width for that decay is given in Eq. C.21b. For example, a 300-GeV Higgs decaying into a pair of 100 GeV W's has a width of about 20 GeV. The width divided by the mass is about 0.07 and this means that the Higgs at this mass is distinguishable as an object that has a width rather less than its mass. As M_H increases, the ratio $\Gamma_H/M_H \sim \alpha(M_H/M_W)^2$ becomes large. This means that a very heavy Higgs (on the scale of M_W) will be unobservable.

How do we produce the Higgs? Well if you recall, $u\bar{d}$ from the $p\bar{p}$ form a W. That process has a cross section which we estimated to be about 10 nanobarns. The Higgs would be formed by $u\bar{u}$ from $p\bar{p}$, a process which has roughly the same differential luminosity. The Higgs cross section for production from light valence fermions would be given in Eq. C.22 (compare to Eq. C.17).

$$\sigma(H) \sim \alpha\left(\frac{M_f^2}{M_W}\right)\left[\frac{\tau}{M^2}\,\frac{dL}{d\tau}\right]_{M = M_H} \qquad \text{C.22}$$

Unfortunately this is a disaster. The cross section is enormously small because, relative to W production, you have a factor of the fermion mass divided by the W mass squared, and that fermion mass refers to the valence quarks. This fact makes the direct mechanism essentially unobservable, due to the low cross section. The most straightforward way to help appears to be to put heavy quarks into a triangle loop as shown in Fig. C.12. This is very much in the spirit of using gluons as flavor blind sources of heavy quarks (as we discussed in Section B). One can think of this as gluon production of heavy quark $Q\bar{Q}$ pairs followed by the fusion of those pairs into the dynamically favored inverse decay of the H^o. The cross section for Higgs production (if $M_H = M_W$) relative to W production can be estimated using Fig. C.12 and Fig. C.1 (as shown in Eq. C.23).

$$\frac{\sigma(H)}{\sigma(W)} = \alpha_s^2 \left(\frac{M_b}{M_W}\right)^2 \quad (L_{gg}/L_{u\bar{d}}) \qquad \text{C.23}$$

Taking the heavy flavor to be the b quark and equating the gg and $u\bar{d}$ luminosity, this factor is 2.5×10^{-5}. Using a W cross section of $10^{-32}cm^2$, then the production cross section for a 100 GeV Higgs boson would be $2.5 \times 10^{-37}cm^2$. A detailed calculation for this process is also shown in Fig. C.12. The estimate is given in Eq. C.24. Clearly the TeV-I collider enjoys an advantage over the SPS collider.

$$\sigma(H) \sim \alpha_s^2 \frac{\alpha}{M_W^2} \left[\tau \frac{dL_{gg}}{d\tau}\right]\left(\frac{M_b}{M_W}\right)^2 \qquad \text{C.24}$$

Assume a luminosity of $10^{30}cm^{-2}sec^{-1}$. A total run span of three years is about 10^8 seconds. Using Fig. C.12, at 100-GeV mass you would get about 100 Higgs over the run. One still has to find a branching fraction which is large and which is experimentally clean so as to dig out these 100 Higgs. At Tev I this analysis means there is clearly an enormous challenge to find the Higgs boson (the object which is

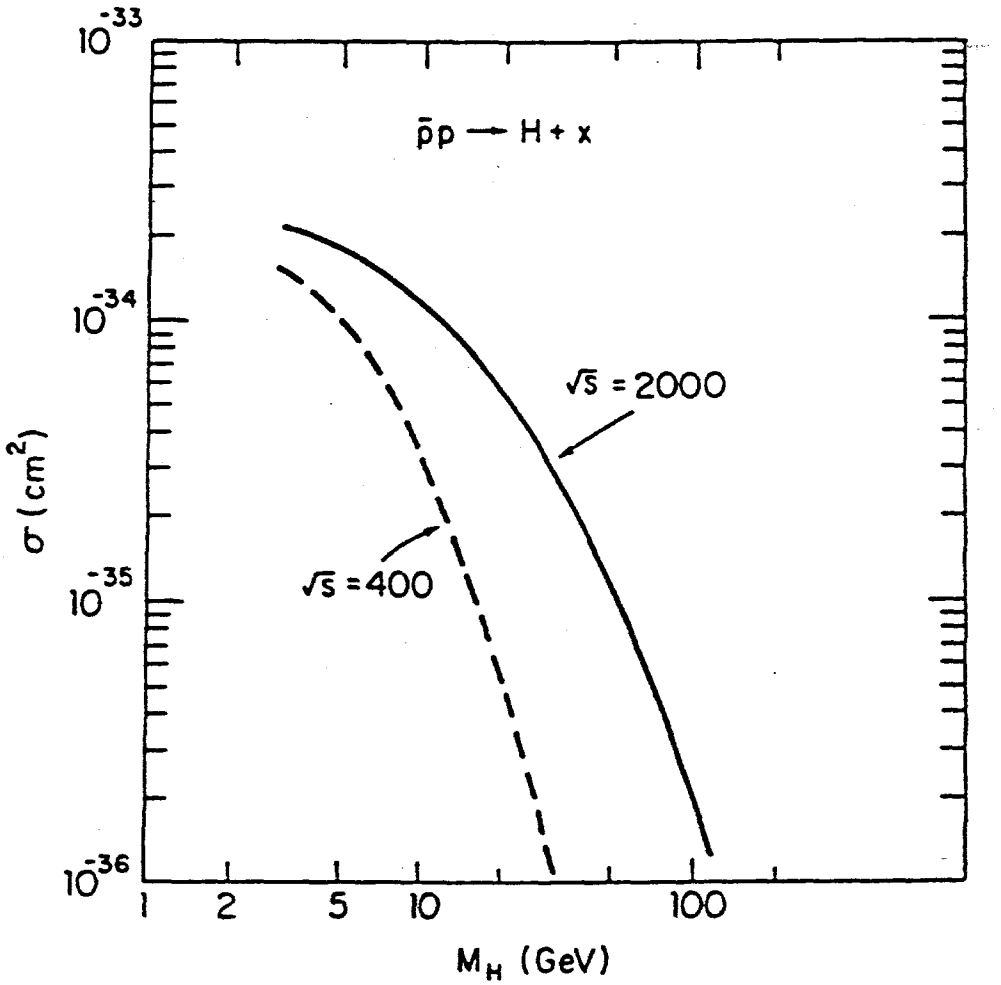

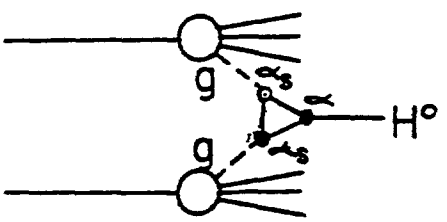

C.12 Predicted cross section for Higgs boson production as a function of the Higgs mass for 2 values of $\sqrt{s}$.

responsible, in a fundamental way, for the electroweak unification). Detection, in an unambiguous way, of such an object is a difficult task at best. It may well be that this will be such an arduous process as to require an improvement program for the accelerator, for the $\bar{p}$ source, for the ultimate luminosity, and also to demand an improvement program for the detectors (to be upgraded in such a fashion that they can utilize this luminosity). It is then barely possible that the Fermilab Collider could find the Higgs scalar, assuming branching modes exist which are recognizable.

Hadron production cross section summary

In summary, let us recall the relative values of the cross sections. σ_T will be $\sim 7.5 \times 10^{-26} cm^2$ (75 mb). If the proton remains gray then we expect $\sigma_{EL}/\sigma_T \sim 1/4$, and $\sigma_D \sim \sigma_{EL}/4$ with elastic and diffractive cross sections of 5 to 20 mb. The remaining $\sigma_I \sim 50$ mb of inelastic cross section will be mostly due to soft ln(s) multiparticle physics. If the soft nature of these events persists, then the single particle cross section to exceed $P_\perp^{MIN}$ is (see Eq. A.15).

$$\sigma(P_\perp > P_\perp^{MIN}) \sim (\rho \sigma_I \Delta y)\left(\frac{2\, P_\perp^{MIN}}{\langle P_\perp \rangle} + 1\right) e^{\frac{-2P_\perp^{MIN}}{\langle P_\perp \rangle}} \qquad \text{C.25}$$

For density ρ=5, rapidity span $\Delta y = 6$, and $\langle P_\perp \rangle = 0.5$ GeV, then with $P_\perp^{MIN} = 4$ GeV,

$$\sigma(P_\perp > 4) \sim 2.9\ \mu b \qquad \text{C.26}$$

Soft processes are, at this $P_\perp$ value, suppressed by ~ 4 orders of magnitude.

In contrast, jets have a cross section (see Eqs. B.8 and B.9), $\hat{\sigma} \sim \alpha_s^2/\hat{s}$. For M = 16 GeV. $P_\perp \sim 8$ GeV, $k_\perp \sim 4$ GeV, and then $\hat{\sigma} \sim 0.016\ \mu b$. The gluon flux, however, is large at these small masses (see Eq. B.17), so that $\sigma(k_\perp > 4$ GeV$) \sim 6\ \mu b$. This checks

with Fig. B.8 and means that jets begin to emerge from the soft debris (at the Collider) at masses of only 16 GeV. This situation is in marked contrast to Fixed-Target experiments where jets are hard to see. Because of the power law behavior of $\hat{\sigma}$ and the rising gluon flux with increasing s (at fixed M, τ decreases), jets will arise more markedly from the ln(s) debris at increased s. The phenomena is analogous to going from SPEAR "jets" to PETRA jets.

Electroweak processes are down with respect to strong processes by a factor (see Eqs. B.13 and C.8) ~ $(\alpha/\alpha_s \sin^2\theta_W)^2$. At TeV-I, gauge boson production is at the 10 nb level, which is about 1000 times smaller than the cross section level where jets begin to become apparent. At a fixed mass M (or $P_\perp$), jets are ~ 1,000 times more copious than leptons from W or Z^o. However single particles from jets are only ~ 30 times more copious, while leptons (from heavy flavor decay) are <u>less</u> copious by a factor $\gtrsim$ 10. Hence, leptons are the key to easily observing gauge bosons.

Gauge boson pairs are down from single gauge bosons by α. At the hadron colliders, jets have come of age in that they now stand out well above the soft hadronic junk. Leptons are so-far the key to digging out the W and Z which are buried in jets by a factor of 1,000:1. The challenges at TeV-I will be to dig out hadronic decays of W and Z, gauge boson pairs, and Higgs. Of course, new phenomena would not be spurned either.

Missing transverse momentum

An example which connects the 3 different regimes and points beyond them is illustrated in Fig. C.13. This figure shows the differential cross section for missing $P_\perp$. Armed with all our previous analyses we can easily understand this distribution. At low $P_\perp$, we see soft processes characterized by exponential falloff with $P_\perp$. A finite sized beam pipe (say $\theta > 1^o$) means, using Eq. A.11, that $|\eta| <$

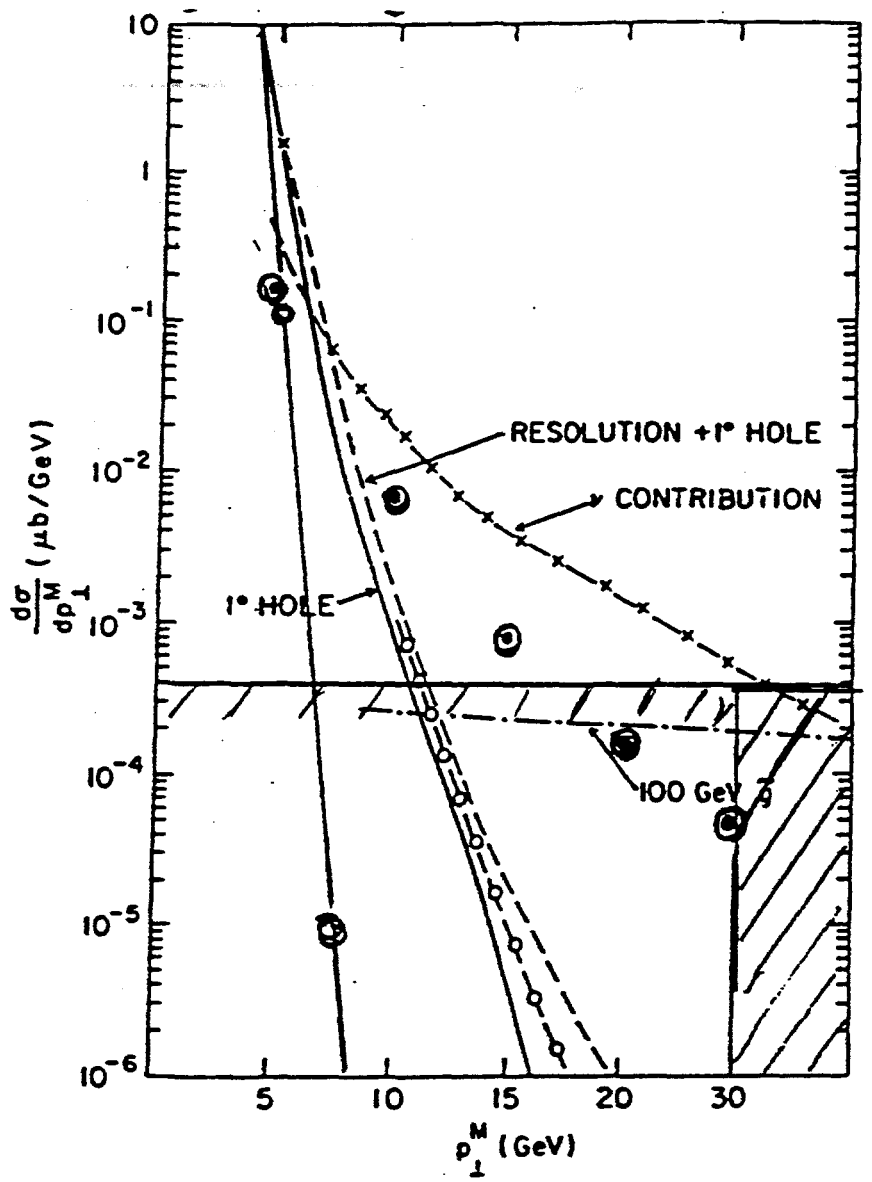

C.13 Differential cross section for missing transverse momentum. The curves are the DØ Monte Carlo results. Circles and shaded regions are crude estimates as described in the text due to soft processes, heavy flavor decays, gauge boson decays, and gluino decays.

4.7. The colliding beams, from Eq. A.9, have $y_{MAX} = 7.7$. This means that a 1° beam pipe loses 6 units of rapidity, three on each side. If we use Eq. A.15 as an estimate, then the open circles plotted in Fig. C.13 are the result. Clearly, any hard beam jets in the pipe exceed the simple estimate for $P_{\perp} > 5$ GeV as might be expected.

For $P_{\perp} > 5$ GeV, the soft processes die off. At higher $P_{\perp}$, neutrinos from heavy flavors are most important for missing $P_{\perp}$. Using the e spectrum of Fig. C.2, multiplying by 3 for ν from $e\nu$, $\mu\nu$, and $\tau\nu$ (asuming universality) and by 4 (for Δy), results in the filled circles shown in Fig. C.13. This contribution of ν to missing $P_{\perp}$ is well estimated in this simple fashion, and dominates from $5 \lesssim P_{\perp} \lesssim 20$ GeV. This region can be considered to be the jet regime.

At still higher values of $P_{\perp}$, $30 \lesssim P_{\perp} \lesssim 40$ GeV, we use our previous estimates (Fig. C.2) for e from W. They are multiplied by 3 ($e\nu$, $\mu\nu$, $\tau\nu$) and by 4 (Δy). A final factor of 1.5 comes from $Z \to \nu\bar{\nu}$ (with 1/8 branching fraction from Eq. C.4, two final state neutrinos, and 1/2 the W cross section from Fig. C.1). This estimate of gauge boson contributions to ν is shown shaded in Fig. C.13. In the region $30 \lesssim P_{\perp}$ 40 GeV it dominates the missing $P_{\perp}$ distribution. The crude estimate is adequately accurate. The last regime is the electroweak. Beyond it ($P_{\perp} > 40$ GeV) is terra incognita.

Gluino production

A new signal one might look for would be the gluino, supersymmetric partner of the gluon. The production cross section can be estimated from the gluon-jet cross section. For a mass of the gluino of 100 GeV, the 200 GeV jet-jet cross section ($\Delta y = 4$) for all jets above that mass is $9.6 \times 10^{-32} cm^2$. Assuming 1/5 of all jets above threshold are gluinos, and that the three-body gluino decay is uniform in $P_{\perp}$ from

zero to $M_{\tilde{g}}/2$ = 50 GeV, one has the shaded estimate, $d\sigma/dP_{\perp} = 4 \times 10^{-34} cm^2/GeV$ shown in Fig. C.13. Again, the full Monte Carlo results are quite close to this crude estimate. This object should appear above backgrounds for missing $\underline{P}_{\perp}$ in excess of 40 GeV, i.e., beyond the electroweak regime in $P_{\perp}$. A goal of the TeV-I physics program will be to push the detectable range of $\underline{P}_{\perp}$ "beyond the electroweak" range in search of new phenomena.

Summary

We have made a cursory pass through Fermilab Collider Physics. Our goal has been to estimate processes (good to an order of magnitude) by hand. Although the brave new world of ISAJET Monte Carlo has arrived, it is still possible to sit down and think through the physics and then make an "abacus estimate".

First "soft physics" was discussed. The elastic cross section is ~ 1/4 of the total indicating that the proton is gray, neither black nor transparent. Diffraction consists of another few mb of σ_T. The remaining inelastic cross section (σ_I) is dominated by soft processes characterized by a "temperature" $\langle P_\perp \rangle$ which defines the production weight ($\exp(-2\, P_\perp / \langle P_\perp \rangle)$). These processes dominate up to $P_\perp \sim 3$ GeV when the cross section is ~ 10 μb.

Beyond $P_\perp \sim 3$ GeV hard scattering processes are important. They are characterized by subprocesses among point constituents which have cross sections which go as $1/\hat{s}$. The sources of the point constituents are defined by distribution functions of the longitudinal momentum fraction x. Armed with the "flux" and the cross section, estimates of $\bar{p}p$ reaction rates can be made. Successful estimates of yields of vector mesons, heavy flavors, and jets have been made. Scaling properties for all these processes are noted and confirmed by the data. A crude relationship of parent/daughter is shown to be approximately valid. Finally, appealing to Section A on soft processes, we estimated the phase space populated by decay products of the partons. These estimates, confirmed by "LEGO" plot data, were used to conceptually design the "towers" for a generic Collider detector.

Finally, hard scattering of electroweak bosons was examined. The electroweak unification means that $g_W \sim e$. The widths and masses of gauge bosons were roughly estimated. The $W^\pm$ and Z^0 branching fractions were found by simple color counting. The production cross section was estimated using the previous vector meson formula,

the differential luminosity for $u\bar{d}$, and the exact EHLQ formula. The estimates were quite good. Backgrounds due to jets were accurately estimated, and smearings due to $W\to\tau\nu$ were mentioned. The data on the x distribution for W's was well reproduced as was the decay angular distribution of $W\to\mu\nu$. The e^+e^- background due to jets was well estimated by the same arguments that were used for estimating $e^\pm$ backgrounds. The Drell-Yan process was discussed, scaling properties were noted, and the Z^o background was estimated. Finally the Z^o rate itself was simply predicted. Data from UA1 confirms the expected cleanliness of the process.

New processes to be observed were mentioned within the context of the standard model. $W\to t\bar{b}$ decays were guesstimated. Like-sign dileptons are expected in the standard model, so that any new phenomena may be buried in "old physics." Production rates for electroweak gauge-boson pairs were calculated. Improved luminosity would obviously be of benefit in this class of physics. Rates and decay modes for the H^o were looked at. Detection of H^o at TeV-I will certainly be a challenge. The missing $p_\perp$ spectrum was discussed and well explained in elementary terms. All possible physics beyond the standard model is beyond the scope of these lectures and can be found in EHLQ.

Acknowledgments

Special thanks go to T.B.W. Kirk for instigating the writing of this text and for providing a critical reading of the text. Also, thanks to T. Gourlay for several proofreadings of the text. Most importantly, thanks to M. Bennett for her patience in typing (and multiple retyping) this manuscript.

References

A.1 Chris Quigg, Gauge Theories of the Strong, Weak, and Electromagnetic Interactions,

Benjamin Publishing Co. (1983).

A.2 F.E. Close, An Introduction to Quarks and Partons, Academic Press (1979).

A.3 E. Leader and E. Predazzi, An Introduction to Gauge Theories and the New Physics, Cambridge University press (1982).

A.4 Review of Particle Properties, Particle Data Group, Rev. Mod. Phys. 56, 2 (1984).

B.1 E. Eichten, I. Hinchliffe, K. Lane, C. Quigg, Supercollider Physics, Rev. Mod. Phys. 56, 4, 579 (1984).

B.2 L. DiLella, Jet Production in Hadronic Collisions, Ann. Rev. Nuc. Part. Sci. 35 (1985).

B.3 Summary Report of the PSSC Discussion Group Meetings, June 1984, Ed. P. Hale, B. Winstein.

C.1 Design Report for the Fermilab Collider Detector Facility (1981).

C.2 Design Report, The DØ Experiment at the Fermilab Antiproton-proton Collider (1984).

C.3 C. Rubbia, Experimental Observation of the Intermediate Vector Bosons W^+, W^-, and Z^o, Rev. Mod. Phys. 57, 3, 699 (1985).